

ON MATVEEV-PIERGALLINI MOVES FOR BRANCHED SPINES

KOHEI MURAMATSU, SAKIE SUZUKI, AND KOKI TAGUCHI

ABSTRACT. The Matveev-Piergallini (MP) moves on spines of 3-manifolds are well-known for their correspondence to the Pachner 2-3 moves in dual ideal triangulations. Benedetti and Petronio introduced combinatorial descriptions of closed 3-manifolds and combed 3-manifolds by using branched spines and their equivalence relations, which involves MP moves with 16 distinct patterns of branchings. In this paper, we demonstrate that these 16 MP moves on branched spines are derived from a primary MP move, pure sliding moves and their inverses. Consequently, we obtain alternative generating sets for the equivalence relations on branched spines for closed 3-manifolds and combed 3-manifolds. Furthermore, we extend these results to framed 3-manifolds and spin 3-manifolds. These descriptions are advantageous, particularly when constructing and studying quantum invariants of links and 3-manifolds. In various constructions of quantum invariants using (ideal) triangulations, branching structures naturally arise to facilitate the assignment of non-symmetric algebraic objects to tetrahedra. In these frameworks, the primary MP move precisely corresponds to certain algebraic pentagon relations, such as the pentagon relation of the canonical element of a Heisenberg double, the Biedenharn-Elliott identity for quantum $6j$ -symbols, or Schaeffer's identity for the Rogers dilogarithm and its non-commutative analog for Faddeev's quantum dilogarithm in quantum Teichmüller theory. We expect our results to contribute to a better understanding of quantum invariants in the context of spines and ideal triangulations.

CONTENTS

1. Introduction	2
1.1. Primary MP move and pure sliding moves on normal o-graphs	2
1.2. Main results	3
1.3. Primary MP move and five term relations arising from quantum invariants	3
1.4. Quantum invariant Z for framed 3-manifolds and cyclic moves	4
1.5. Moves on normal o-graphs and algebraic equations of quantum invariants	4
1.6. Organization of this paper	5
2. Normal o-graphs and combed 3-manifolds	5
2.1. Branched spines and associated vector fields	5
2.2. Normal o-graphs and branched polyhedrons	6
2.3. Closed normal o-graphs and combed 3-manifolds	7
2.4. Pure sliding moves on branched polyhedrons	8
2.5. Pure sliding moves on normal o-graphs	9
2.6. Main results for closed 3-manifolds and combed 3-manifolds	11
2.7. Proof of Theorem 2.3	12
2.8. Local pure sliding moves and refinement of Theorem 2.3	16
3. Integral normal o-graphs and framed 3-manifolds	17
3.1. Branched spines and framed 3-manifolds	17
3.2. Integral normal o-graphs	18
3.3. Framed normal o-graphs and framed 3-manifolds	19
3.4. Euler cochain c_P	20
3.5. Integral pure sliding moves on integral normal o-graphs	20
3.6. Main results for framed 3-manifolds	22
3.7. Local integral pure sliding moves and refinement of Theorem 3.3	22
4. Spin normal o-graphs and spin 3-manifolds	22
A. Symmetry of moves	23
B. Cyclic moves	25
References	27

1. INTRODUCTION

1.1. Primary MP move and pure sliding moves on normal o-graphs. A normal o-graph is a decorated 4-valent graph which represents a branched spine of a 3-manifold, and it can be described by an oriented virtual link diagram. The dual of a branched spine corresponds to a branched ideal triangulation, that is, an ideal triangulation in which the 4 ideal vertices of each ideal tetrahedron are ordered so that when two tetrahedra share a common face the orders are compatible.

A combed 3-manifold is a closed 3-manifold endowed with a combing, that is, a homotopy class of a nowhere-vanishing vector field. Benedetti and Petronio [5] established combinatorial descriptions of closed 3-manifolds and combed 3-manifolds by using normal o-graphs and their equivalent relations involving 16 patterns of the Matveev-Piergallini (MP) moves shown in Figure 1.1.

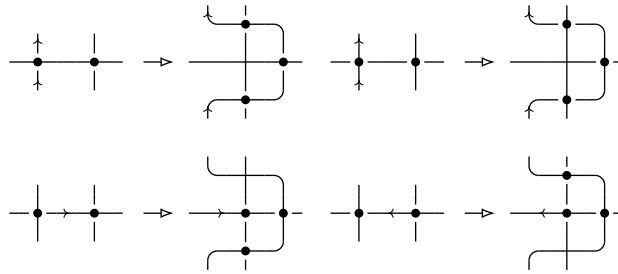


Figure 1.1. MP-moves. Orientation of each non-oriented edge is arbitrary if it matches before and after move.

We introduce the *primary MP move* as in Figure 1.2, which is equivalent to a specific MP move of type D2 (see Figures 2.21 and 2.22). It resembles the Reidemeister III move on knot diagrams, with the key difference being that the left-hand side includes only two real crossings, while the other one is virtual, whereas all three crossings on the right-hand side are real. The primary MP move can be seen as a relation in the set of morphisms in the *category of normal o-tangles* [17], similarly to the Reidemeister moves in the category of tangles, generated as a monoidal category by fundamental diagrams (crossings, maxima and minima).

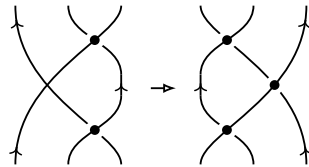


Figure 1.2. Primary MP move.

Consider the boundary surfaces of the branched ideal triangulations corresponding to the branched spines in the primary MP move. The bottom and top part of these surfaces are branched triangulated pentagons and the primary MP move induces a specific pentagon identity involving flip transformations, see Figure 1.3. This pentagon identity on branched triangulated surfaces plays a foundational role in the theory of quantum $6j$ -symbols [14, 24] and quantum Teichmüller theory [1, 6, 13], as well as in the framework of quantum cluster algebras [9, 10].

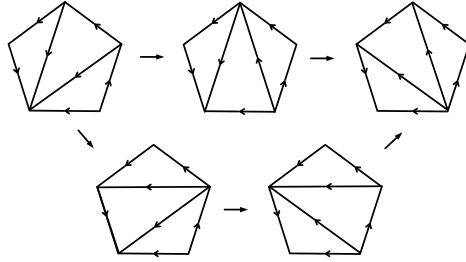


Figure 1.3. Pentagon identity of branched triangulations.

The primary MP move was introduced in [22] as a *colored Pachner (2,3) move*, which was employed to study the universal quantum invariant of links [15, 19] using ideal triangulations of link complements. The MP move of type D2 emerged also in [4] as a *remarkable non ambiguous b-transit*¹, utilized as a generator of a combinatorial description of the *non ambiguous structure* of compact oriented 3-manifolds.

The *pure sliding moves on branched spines* are defined in [5]. We translate this definition into the context of diagrams of normal o-graphs and define the *pure sliding moves on normal o-graphs* as shown in Figure 1.4. These moves can only be performed when a specific global condition is satisfied on the normal o-graphs (see Section 2.5). This condition corresponds to a requirement on the 2-cells of the branched spines (see Section 2.4).

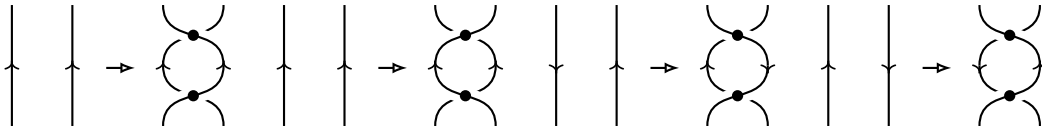


Figure 1.4. Pure sliding moves.

1.2. Main results. In this paper we show that each MP move in Figure 1.1 is derived as a sequence of instances of the primary MP move, the pure sliding moves, and their inverses (Theorem 2.3). Consequently, we have alternative generating sets of the equivalence relations on branched spines for combed 3-manifolds (Corollary 2.4) and closed 3-manifolds (Corollary 2.5). Corollary 2.4 is equivalent to the results in [11, Theorem 2.3] by I. Ishii, where he uses flow spines to represent closed 3-manifolds. His proof contains a geometrical argument involving non-singular flows and local sections in 3-manifolds, while our proof reduces to combinatorial arguments on normal o-graphs (see Remark 2.2).

A framed 3-manifold is a closed 3-manifold with a framing, defined as a homotopy class of a trivialization of the tangent bundle. Benedetti-Petronio [5] also gave combinatorial descriptions of framed 3-manifolds and spin 3-manifolds by using framed normal o-graphs, which are normal o-graphs having a \mathbb{Z}_2 -weight on each edge (see Section 3.2). S. Mihalache, Y. Terashima and the second author [18] used integral normal o-graphs, which, for closed 3-manifolds, are integer lifts of framed normal o-graphs. In the present paper, we introduce pure sliding moves on integral normal o-graphs and show that these moves do not alter the framing of the associated 3-manifolds (Proposition 3.2). Subsequently, we establish results similar to Theorem 2.3 for both integral normal o-graphs (Theorem 3.3) and framed normal o-graphs (Corollary 3.4). As a consequence, we provide alternative generating sets for the equivalence relations for framed 3-manifolds (Corollary 3.5) and spin 3-manifolds (Corollary 4.3).

1.3. Primary MP move and five term relations arising from quantum invariants. In various constructions of quantum invariants using (ideal) triangulations, branching structures naturally arise to facilitate the assignment of non-symmetric algebraic objects to tetrahedra. The primary MP move can be viewed as a topological realization of certain algebraic pentagon relations arising from such quantum invariants. Kashaev [12] showed that a canonical element S of the Heisenberg double of a finite dimensional Hopf algebra satisfies the *pentagon relation* $S_{23}S_{12} = S_{12}S_{13}S_{23}$. The quantum invariant defined in [17, 18, 22]

¹The positive crossing of normal o-graph corresponds dually to a negatively oriented branched tetrahedron. Thus the primary MP move is the remarkable non ambiguous *b-transits* involving only negatively *b*-oriented tetrahedra.

by Mihalache, Terashima, and the second author is constructed based on associating a branched tetrahedron with the canonical element S of a Heisenberg double. This construction is functorial and it maps a real positive crossing of normal \mathfrak{o} -graphs to the canonical element S , and the primary MP move to the pentagon relation $S_{23}S_{12} = S_{12}S_{13}S_{23}$. Through the theory of quantum $6j$ -symbols, the primary MP move corresponds to the *Biedenharn-Elliott identity*. This framework yields in particular the reduced Turaev-Viro invariant [4], which, after symmetrization, recovers the Turaev-Viro invariant [24]. Faddeev’s quantum dilogarithm [8] plays a crucial role in the theory of quantum Teichmüller theory and of complex Chern-Simons theory. This quantum dilogarithm appears in the canonical element of the Heisenberg double of the Borel subalgebra of $U_q(\mathfrak{sl}_2)$. The pentagon relation of Faddeev’s quantum dilogarithm, which is a non-commutative analog of *Schaeffer’s identity* for the classical Rogers dilogarithm, corresponds to the sequence of flip transformations of branched surfaces as shown in Figure 1.3. The quantum hyperbolic invariant [2–4] is similarly defined based on the Heisenberg double, specifically using the $6j$ -symbols for the cyclic representation theory of the Borel subalgebra of $U_q(\mathfrak{sl}_2)$ at a root of unity. In this context, the action of the canonical element on a cyclic irreducible representation is referred to as the *basic matrix dilogarithm*, while the pentagon relation is termed the *matrix Schaeffer’s identity*.

1.4. Quantum invariant Z for framed 3-manifolds and cyclic moves. The quantum invariant Z constructed in [18] using the Heisenberg double of a Hopf algebra H is an invariant of framed 3-manifolds.² When H is involutory, the invariant aligns with that in [22], reducing to a combed 3-manifolds invariant. Additionally, if H is unimodular and counimodular, the invariant simplifies to a topological 3-manifolds invariant constructed in [17]. The proof of invariance of Z requires showing consistency under the 16 MP moves. By employing the primary MP move and the pure sliding moves instead of the 16 MP moves, the proof becomes more straightforward.

The obstruction of Z to be topological invariant, or, in other words, the aspect related to framing, lies in its invariance under “cyclic” moves. These moves involve a region surrounded by edges oriented cyclically, see Figure 1.5 for examples.³

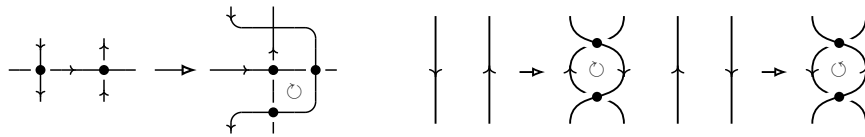


Figure 1.5. Cyclic MP move and cyclic pure sliding moves.

When we use the primary MP move and the pure sliding moves, the obstruction is only the invariance under cyclic pure sliding moves. More precisely, each non-cyclic MP move can be derived as a sequence of instances of the primary MP move and non-cyclic pure sliding moves, whereas any decomposition of a cyclic MP move as a sequence of moves must include at least one cyclic pure sliding move. Thus we can say that the obstruction essentially resides in the cyclic pure sliding moves. See Appendix B for details.

1.5. Moves on normal \mathfrak{o} -graphs and algebraic equations of quantum invariants. One of the most interesting challenges in the study of quantum invariants is understanding the relationship between three-dimensional topology and the algebraic properties of these invariants. In response to Atiyah’s quest for an intrinsically three-dimensional definition of the Jones polynomial, Witten [25] used Chern-Simons theory and three-dimensional topological quantum field theory, paving the way for a possible topological interpretation of the Jones polynomial. This approach also led him to propose new types of 3-manifold invariants. Witten employed a path integral, a concept not rigorously defined in mathematics, yet his theory provided substantial insights. However, a comprehensive understanding within a mathematically rigorous framework remains elusive, and the present paper might take a step towards addressing this gap by establishing a three-dimensional framework for studying generalizations of the Jones polynomial. More precisely, the universal quantum invariant of links [15, 19] recovers the Reshetkhin-Turaev invariants [20] of links, in particular, the colored Jones polynomials. From the universal quantum invariant, we can also construct the Witten-Reshetkhin-Turaev invariant [21] of 3-manifolds. By extending the results in [18, 22], in [23], the second

²In [18], the scope was limited to 3-manifolds with vanishing first Betti number.

³In [18], we classify MP moves of type A and type B, and type B corresponds the set of cyclic MP moves.

author reconstructed the universal quantum invariant for the Drinfeld double using integral normal o-graphs and the invariant Z . In this sense, the invariant Z might incorporate the Reshetkhin-Turaev invariant of links (as invariants of link complements with framings) and a framing refinement of the Witten-Reshetkhin-Turaev invariant. The description of 3-manifolds using the primary MP move and the pure sliding moves aligns with the invariant Z , where the correspondence between topological phenomena and algebraic structure through the invariant is straightforward and comprehensible; a crossing of a normal o-graph (or an ideal tetrahedron in the dual ideal triangulation) corresponds to the canonical element; the primary MP move (or the Pachner 2-3 move) embodies the pentagon relation of the canonical element, while the pure sliding moves (or the Pachner 0-2 moves) reflect its invertibility. In this harmonious correlation, understanding the moves of normal o-graphs implies understanding the corresponding algebraic equations of the invariants. We expect our results to contribute to a better understanding of quantum invariants in the context of spines and ideal triangulations.

1.6. Organization of this paper. The paper is organized as follows. We start by discussing the description of combed 3-manifolds and closed 3-manifolds in Section 2. Here, we revisit the definition of branched spines in Section 2.1 and explain a one-to-one correspondence between branched spines and normal o-graphs in Section 2.2. In Section 2.3, we recall the combinatorial description of combed 3-manifolds and closed 3-manifolds using closed normal o-graphs. We then transition to the study of the pure sliding moves, initially we recall the original definition from [5] on branched spines in Section 2.4, and subsequently we introduce its combinatorial realization on normal o-graphs in Section 2.5. Our main results, outlined in Section 2.6, are detailed, with corresponding proofs provided in Section 2.7. The discussion extends to local pure sliding moves in Section 2.8. We then focus on framed 3-manifolds and integral normal o-graphs in Section 3. Here, in Sections 3.1 and 3.2, we recall the description of framed 3-manifolds using branched spines and integral normal o-graphs. We then recall the combinatorial description of framed 3-manifolds using framed normal o-graphs in Section 3.3. In subsequent sections, including Sections 3.4 and 3.5, we introduce integral pure sliding moves and investigate their impact on framings. Our main results regarding framed 3-manifolds are presented in Section 3.6, with a further refinement provided in Section 3.7. In Section 4, we give the results for spin normal o-graphs and spin 3-manifolds. The appendices provide further analyses, including an investigation into the symmetries of the MP moves in Appendix A, and a study of cyclic moves in Appendix B.

Acknowledgments. We would like to thank Yuya Koda and Serban Matei Mihalache for valuable discussions. This work is partially supported by JSPS KAKENHI Grant Number JP19K14523.

2. NORMAL O-GRAPHS AND COMBED 3-MANIFOLDS

In what follows 3-manifolds are always connected, compact and oriented, with or without boundary. In Sections 2.1–2.3, we follow the notation in [18].

2.1. Branched spines and associated vector fields. For an introduction to standard and branched spines, see e.g. [5, 16]⁴. A 2-dimensional compact polyhedron P is called *simple* if the neighborhood of each point $x \in P$ is homeomorphic to one of the pictures in Figure 2.1, where from the left in the picture the point x is called a *non-singular point*, a *triple point*, and a *true vertex*, respectively.

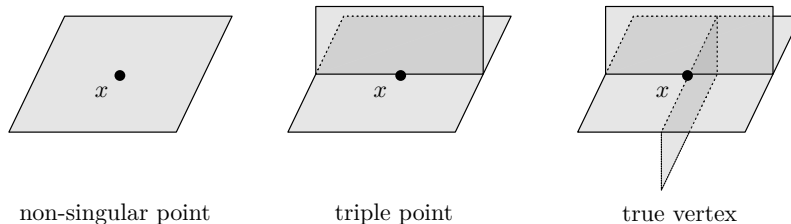


Figure 2.1. Neighborhood of point in P .

⁴In [16], standard spine is called special spine.

For a simple polyhedron P , set

$$\begin{aligned} V(P) &= \{x \in P \mid x \text{ is a true vertex}\}, \\ S(P) &= \{x \in P \mid x \text{ is a true vertex or a triple point}\}, \\ D(P) &= \{x \in P \mid x \text{ is a non-singular point}\}. \end{aligned}$$

A simple polyhedron P is called *standard* if connected components of $S(P) \setminus V(P)$ and $D(P)$ are 1-cells and 2-cells, respectively. Let M be a 3-manifold with non-empty boundary. A standard polyhedron P embedded in $\text{Int}M$ is called a *standard spine* of M if M collapses to P . It is known that every compact 3-manifold with non-empty boundary admits a standard spine. A standard spine P of M determines the homeomorphism class of M , i.e., if P' is a standard spine of M' which is homeomorphic to P , then M' is homeomorphic to M .

An *oriented standard polyhedron* is a standard polyhedron which is a spine of an oriented 3-manifold [5, Proposition 2.1.2]. An *oriented branching* on an oriented standard polyhedron P is an orientation on its 2-cells such that on each 1-cell, the orientations induced from the 2-cells attached to it are not compatible, i.e., there are locally three 2-cells which are attached to a 1-cell e and one of the three induced orientations on e is opposite to the other two (cf. [5, Corollary 3.1.7]). We can visualize a branching structure on P as a smoothing of P as shown in Figure 2.2, where the “branching” starts from the region which induces inverse orientation on the 1-cell relative to the others. Here, each 1-cell has a canonical orientation as the two compatible orientations induced by the 2-cells attached to it. Up to orientation-preserving homeomorphism, there exist two possibilities for the branching structure near the 0-cell, the *type +* and the *type -*, which are shown in Figure 2.3.

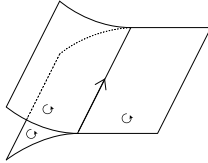


Figure 2.2. Branching.

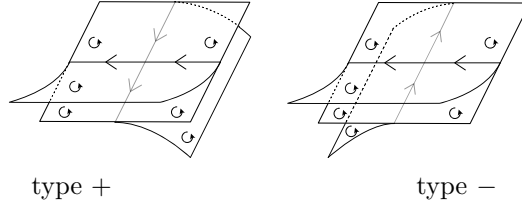


Figure 2.3. Local branching near true vertex.

By abusing the terminology, we refer to an oriented standard polyhedron with an oriented branching as a *branched polyhedron*. Let P be a branched polyhedron and $M(P)$ the 3-manifold obtained by thickening P . Then P defines a unique nowhere-vanishing vector field $v(P)$ on $M(P)$, perpendicular to P and following a right-hand screw direction as depicted in Figure 2.4.

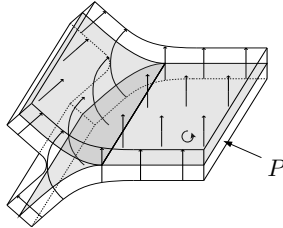


Figure 2.4. Vector field on $M(P)$.

2.2. Normal o-graphs and branched polyhedrons. A *normal o-graph* is an oriented virtual link diagram up to planar isotopy and Reidemeister type moves defined in Figure 2.5.

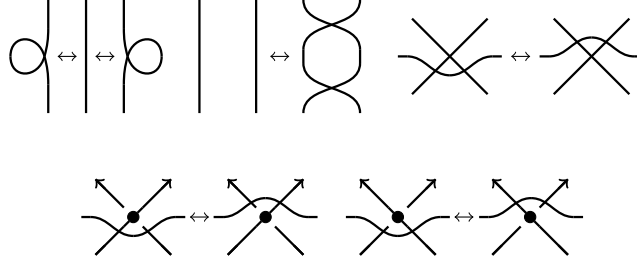


Figure 2.5. Reidemeister type moves.

A normal o-graph represents a branched polyhedron in a combinatorial manner. For a branched polyhedron P , we replace each true vertex with a real crossing in \mathbb{R}^2 ; we replace each vertex of type $+$ or $-$ to a positive or negative crossing, respectively, see Figure 2.6.

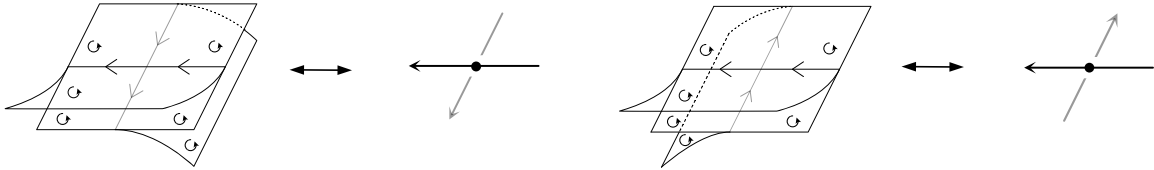


Figure 2.6. Correspondence between branched polyhedron and virtual link diagram near vertex of Type $+$ (left) and type $-$ (right).

Then we obtain a normal o-graph by connecting them according to how the true vertices are connected. Note that this construction is unique up to planer isotopy and the Reidemeister type moves.

Conversely, we can construct in a natural way from an oriented virtual link diagram a homeomorphism class of a branched polyhedron. As a result, homeomorphism classes of branched polyhedra correspond one-to-one with normal o-graphs. In the following discussion, we occasionally treat branched polyhedra and normal o-graphs interchangeably.

2.3. Closed normal o-graphs and combed 3-manifolds. We recall from [5] the presentations of combed 3-manifolds and closed 3-manifolds.

Let M be a closed 3-manifold. A *combing* v of M is a nowhere-vanishing vector field over M . A combed 3-manifold is a pair (M, v) of a closed oriented 3-manifold M and its combing v . Two combed 3-manifolds (M, v) and (M', v') are *equivalent* if there exists an orientation-preserving diffeomorphism $h: M \rightarrow M'$ such that h_*v is homotopic through combings to v' . We denote by $\mathcal{M}_{\text{comb}}$ the set of equivalent classes of combed 3-manifolds.

Note that for a branched polyhedron P , the vector field $v(P)$ of $M(P)$ induces a stratification $\partial M = \partial_{\text{out}}M \cup \partial_{\text{tan}}M \cup \partial_{\text{in}}M$ on the boundary of $M(P)$, where

$$\begin{aligned} \partial_{\text{out}}M &= \{x \in \partial M \mid \text{the field } v \text{ at } x \text{ points outward}\}, \\ \partial_{\text{tan}}M &= \{x \in \partial M \mid \text{the field } v \text{ at } x \text{ is tangent to } \partial M\}, \\ \partial_{\text{in}}M &= \{x \in \partial M \mid \text{the field } v \text{ at } x \text{ points inward}\}, \end{aligned}$$

as shown in Figure 2.7. A *closed branched polyhedron* P is a branched polyhedron such that $\partial M(P)$ is diffeomorphic to the 2 dimensional sphere $S^2 = \{(x, y, z) \in \mathbb{R}^3 \mid x^2 + y^2 + z^2 = 1\}$ with the stratification given by $\partial_{\text{out}}S^2 = \{z < 0\}$, $\partial_{\text{tan}}S^2 = \{z = 0\}$, $\partial_{\text{in}}S^2 = \{z > 0\}$. For a closed branched polyhedron P , the associated vector field $v(P)$ on $M(P)$ extends to the combing $\widehat{v}(P)$ of closure $\widehat{M}(P)$ of $M(P)$ by capping the S^2 boundary with a ball having the trivial flow $(B^3, \frac{\partial}{\partial z})$.

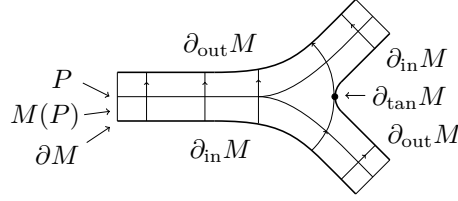


Figure 2.7. Stratification of boundary of $M(P)$.

A *closed normal o-graph* is a normal o-graph which represents a closed branched polyhedron. We denote by \mathcal{G} the set of closed normal o-graphs. See Figure 2.8 for examples of closed normal o-graphs representing the Lens spaces $L(p, 1)$ for $p \geq 0$, where the normal o-graph contains p true vertices.



Figure 2.8. Normal o-graph representing Lens space $L(p, 1)$.

The above construction defines a map

$$\Phi_{\text{comb}}: \mathcal{G} \rightarrow \mathcal{M}_{\text{comb}}, \quad \Gamma \mapsto (\widehat{M}(\Gamma), \widehat{v}(\Gamma)),$$

which is in fact surjective [5, Proposition 5.2.3].

Proposition 2.1 (Benedetti-Petronio [5, Theorem 1.4.1]). The equivalence relation defined by Φ_{comb} is generated by the 0-2 *move* defined in Figure 2.9 and the MP moves defined in Figure 1.1.

We denote by \mathcal{M} the set of closed 3-manifolds up to orientation-preserving diffeomorphism. We have a surjective map

$$\Phi: \mathcal{G} \rightarrow \mathcal{M}, \quad \Gamma \mapsto \widehat{M}(\Gamma).$$

Proposition 2.2 (Benedetti-Petronio [5, Theorem 1.4.2]). The equivalence relation defined by Φ is generated by the 0-2 move, the MP moves, and the *CP move* defined in [5, Figure 1.6]⁵.

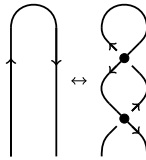


Figure 2.9. 0-2 move.

2.4. Pure sliding moves on branched polyhedrons. The *pure sliding moves* on branched polyhedrons are introduced in [5, Figure 4.7], which is defined as in Figure 2.10.⁶

⁵We will not show the figure of the CP move because we do not use it in this paper.

⁶Note that pure sliding moves I and II have the same configuration after rotation, but the orientations of 2-cells do not match. In [5, Figure 4.7], both pure sliding moves I and II are depicted with a single picture, whereas we distinguish between them by considering the orientations of 2-cells.

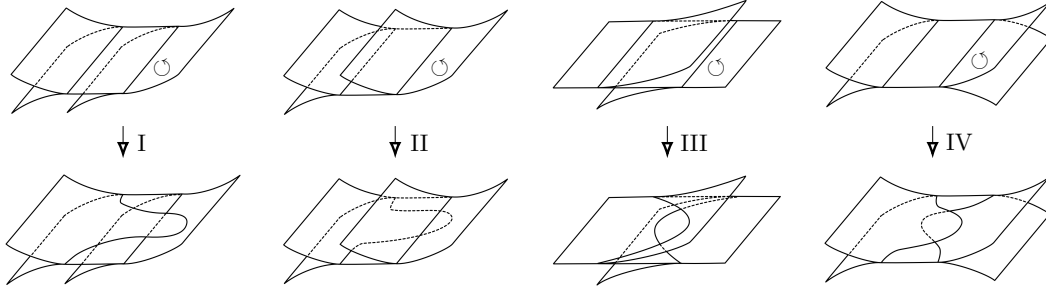


Figure 2.10. Pure sliding moves I-IV on branched polyhedrons.

It is not difficult to check that the 0-2 move is a pure sliding move. We should emphasize that we cannot represent the pure sliding moves solely using a diagram of two edges of a normal o-graph, because such local diagram does not cover the global information about the arrangement of 2-cells, see Figure 2.11 for example.

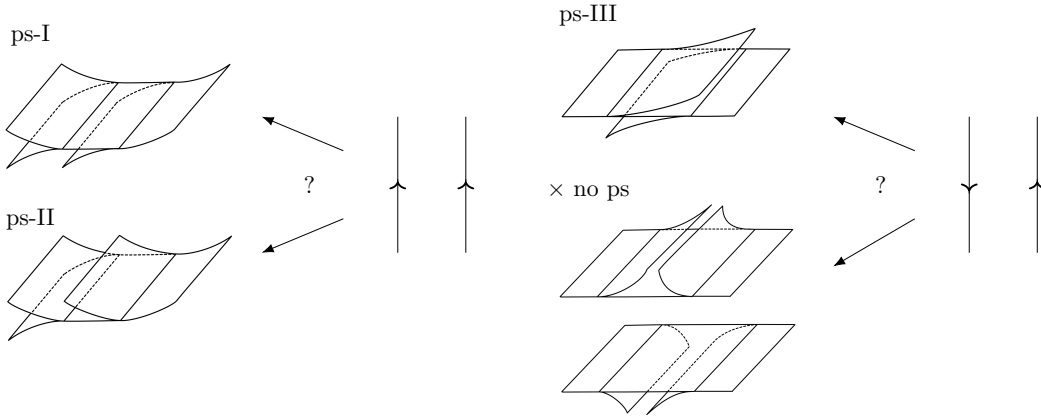


Figure 2.11. Possible configurations of branched polyhedra arising from local edges of normal o-graphs.

In the next section we will give a combinatorial method for performing the pure sliding moves on normal o-graphs.

2.5. Pure sliding moves on normal o-graphs. To implement the pure sliding moves on normal o-graphs, it is necessary to consider 2-cells within a branched polyhedron. Let Γ be a normal o-graph and P the corresponding branched polyhedron. Benedetti and Petronio ([5, Figure 1.3]) introduced a procedure (Method A) to associate a union of circuits with a normal o-graph Γ , as illustrated in Figure 2.12. These circuits represent the boundaries of 2-cells and their attaching maps to the 1-skeleton $S(P)$.

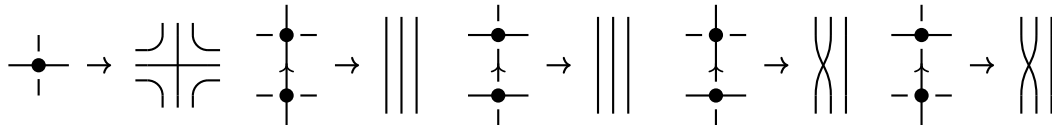


Figure 2.12. Method A.

We slightly modify their method as follows: we replace the neighborhood of each true vertex, as shown in Figure 2.13, and connect them along edges using parallel curves (Method B). It is important to note that Method A and Method B convey the same information regarding 2-cells and their attaching maps.

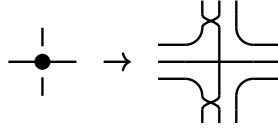


Figure 2.13. Method B.

An advantage to use Method B is that the procedure is functorial⁷, where we replace neighborhoods of true vertices and edges independently, while with Method A the circuit diagram around an edge depends on the two true vertices on the boundary of the edge. Another advantage, which is essential in the following argument, is that the following orders are consistent;

- the order of three lines in the circuit diagram around an edge: we count from left to right seeing the edge of normal o-graph going upwards, and
- the order of three (local) 2-cells at the triple line: we count by the right-hand screw order which ends the 2-cell starting the branching,

see Figure 2.14. Note that if there appears a crossing in the circuit diagram around an edge, as in Method A, then the order is broken at some point.

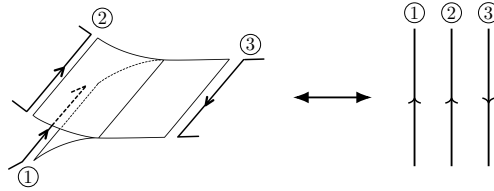


Figure 2.14. Correspondence between configuration of 2-cells around triple line and lines in circuit diagram.

Method B of circuit diagrams enables us to define the pure sliding moves combinatorially on normal o-graphs as follows.

A *pure sliding move* on normal o-graph is defined as in Figure 2.15, where the normal o-graph before we perform each move ps-I – ps-IV should respectively satisfy the following condition: on the circuit diagram by Method B, around the two edge where we perform the move, we have

- (PS-I) the third line on the left is connected to the second line on the right,
- (PS-II) the third line on the left is connected to the first line on the right,
- (PS-III) the first line on the left is connected to the second line on the right,
- (PS-IV) the third line on the left is connected to the third line on the right,

see Figure 2.16.

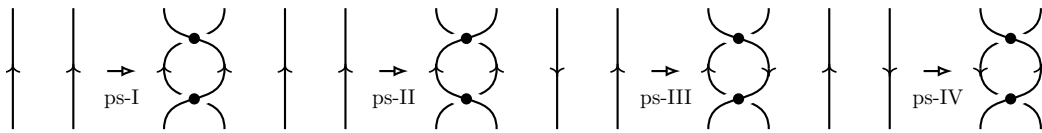


Figure 2.15. Pure sliding move ps-I – ps-IV.

⁷We can describe it as a functor between certain categories.

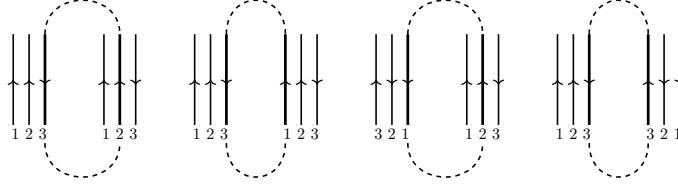


Figure 2.16. Conditions (PS-I)– (PS-IV) for ps-I – ps-IV, respectively.

One can verify that each condition (PS-I)–(PS-IV) corresponds to the connection of the 2-cells involved in the pure sliding moves I–IV on the branched spine. For example, when we count the parts of the 2-cells in branched polyhedron involved in the pure sliding move I as in the right in Figure 2.17, then the Δ_3 is attached to the third strand on the left on the circuit diagram, and to the second on the right.

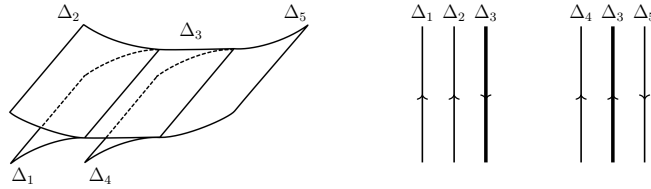


Figure 2.17. Configuration of branched polyhedron on which we perform pure sliding move I (left) and condition for performing ps-I on normal o-graph (right).

Remark 2.1. The pure sliding moves on normal o-graphs are local in the sense that the normal o-graph does not change the out of the sliding region, but is not local in the sense that we need global information to check the conditions (PS-I)–(PS-IV). In Section 2.8 we define local pure sliding moves on normal o-graphs, which are local in both of the above sense.

2.6. Main results for closed 3-manifolds and combed 3-manifolds. We state the main results for closed 3-manifolds and combed 3-manifolds. The proof of Theorem 2.3 will be presented in the next section.

Theorem 2.3. Each of the 16 MP moves in Figure 1.1 is derived as a sequence of the primary MP move in Figure 1.2, the pure sliding moves in Figure 2.15, and their inverses.

Consequently we can replace the 16 MP moves in the equivalence relation for Φ and Φ_{comb} in Propositions 2.1 and 2.2 by the primary MP move and the pure sliding moves.

Corollary 2.4. The equivalence relation defined by the surjective map $\Phi_{\text{comb}}: \mathcal{G} \rightarrow \mathcal{M}_{\text{comb}}$ is generated by the primary MP move and the pure sliding moves.

Corollary 2.5. The equivalence relation defined by the surjective map $\Phi: \mathcal{G} \rightarrow \mathcal{M}$ is generated by the primary MP move, the pure sliding moves and the CP move.

Remark 2.2. Corollary 2.4 are equivalent to [11, Theorem 2.3] by Ishii, where he used flow spines for closed 3-manifolds. His proof contains methods involving non-singular flows and local sections in 3-manifolds, while our proof contains only combinatorial argument on normal o-graphs (after admitting the results in [5]). The first regular moves R_1 in [11] corresponds to *the primary MP move negative*, that is, the primary MP move with each crossing replaced by negative crossings, and the inverse of the second regular moves $R_2-(x), x = 1, 2, 3, 4$, correspond to the pure sliding moves. The “regular equivalence” in [11] corresponds to the equivalence relation on closed normal o-graphs generated by the primary MP move negative and the four moves in Figure 2.15 without condition (PS-I)–(PS-IV), and “strongly regular equivalence” corresponds equivalence relation generated by the primary MP move negative and moves in Figure 2.15 requiring involved normal o-graphs to be closed. This condition is combinatorially nothing but the conditions (PS-I)–(PS-IV). Note also that Theorem 2.3 works for not only closed normal o-graphs but also arbitrary normal o-graphs representing 3-manifolds with boundary.

2.7. Proof of Theorem 2.3. We prove Theorem 2.3. We classify the 16 MP moves into four types A, B, C, D depending on their shape, and then label 1, 2, 3, 4 in each type depending on the orientation of the two edges with arbitrary orientation, see Figure 2.18-2.21.

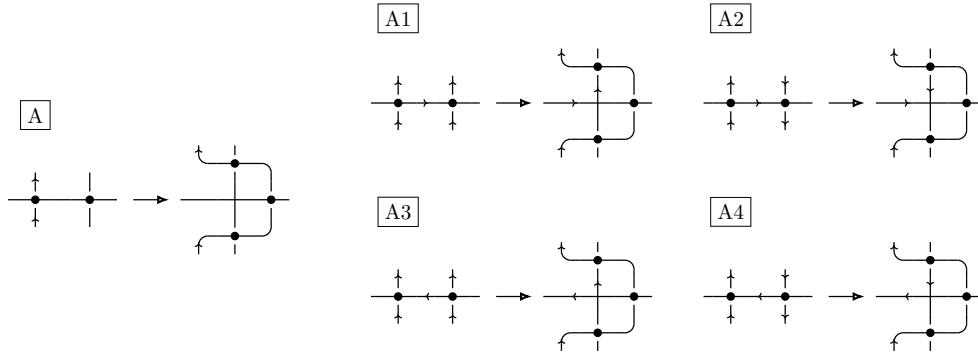


Figure 2.18. MP moves of type A.

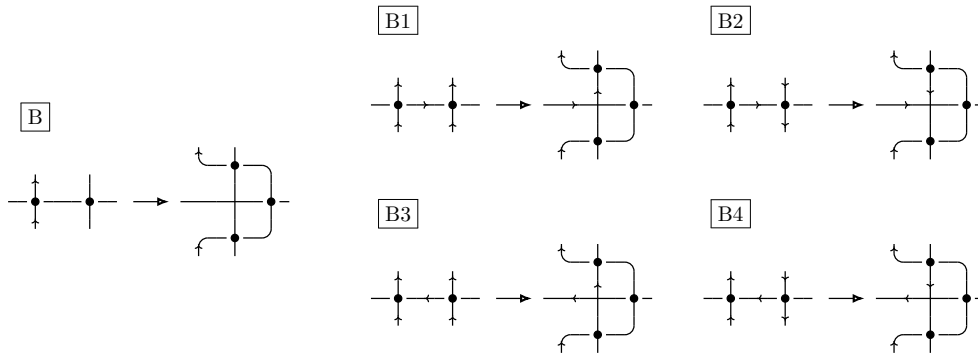


Figure 2.19. MP moves of type B.

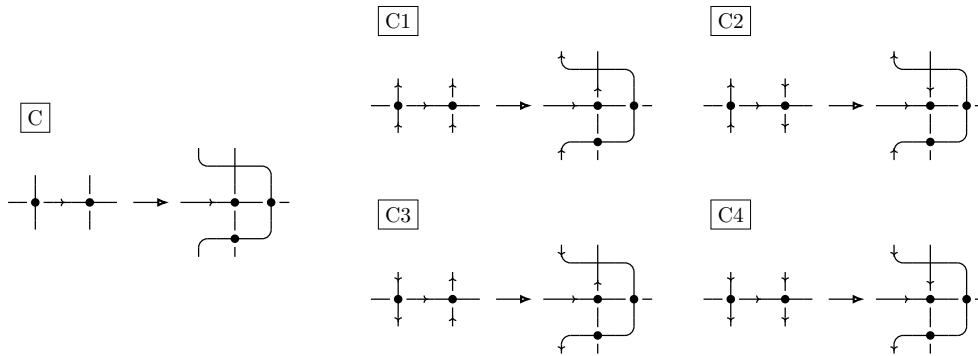


Figure 2.20. MP moves of type C.

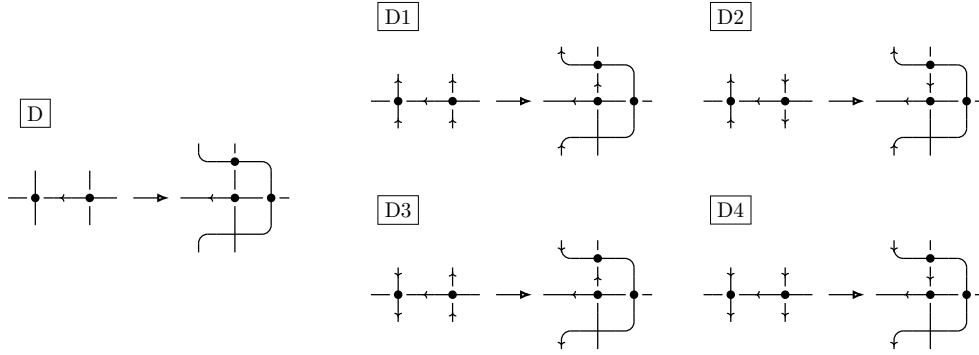


Figure 2.21. MP moves of type D.

The primary MP move is equivalent to D2 as in the following figure.

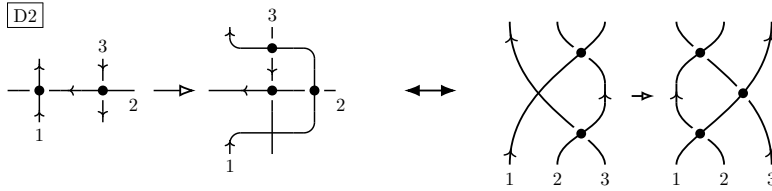


Figure 2.22. Correspondence between D2 and primary MP move.

Thus we will prove that each MP move is derived as a sequence of D2, the pure sliding moves, and their inverses.

See the following figure.

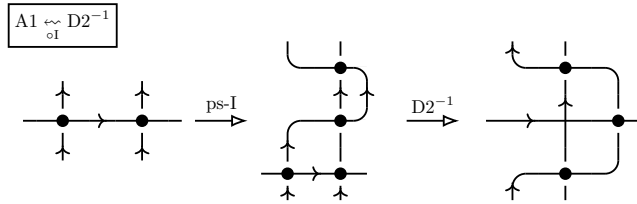


Figure 2.23. A1 is sequence of $D2^{-1}$ and ps-I.

The left picture and the right picture are normal o-graphs before and after performing A1, and thus A1 is derived as a sequence of the ps-I and $D2^{-1}$ in this order. In this case, we denote by $A1 \overset{\circlearrowleft}{\underset{\circlearrowright}{\circ}} D2^{-1}$ standing for “A1 = $(D2^{-1}) \circ (\text{ps-I})$ ” regarding moves as maps. Here, we can check the condition (PS-I) as in Figure 2.24 for performing the first ps-I.

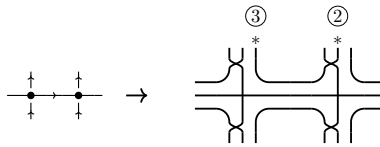


Figure 2.24. Confirming condition (PS-I).

When $A1 \overset{\circlearrowleft}{\underset{\circlearrowright}{\circ}} D2^{-1}$, we also have $A1^{-1} \overset{\circlearrowleft}{\underset{\circlearrowright}{\circ}} D2$ which stands for “ $A1^{-1} = (\text{ps-I})^{-1} \circ (D2)$ ”, following Figure 2.23 inversely. We will use similar notations also for other types of the MP moves.

Lemma 2.6. We have the following relations among the MP moves and their inverses.

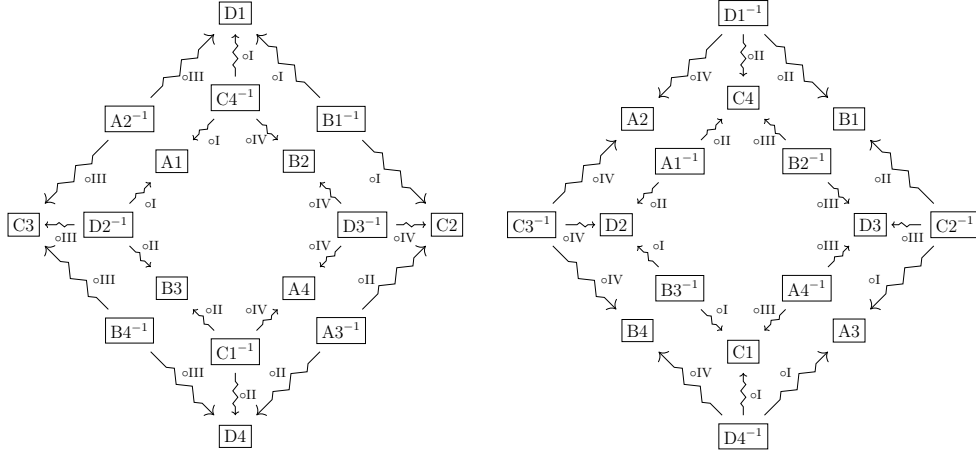


Figure 2.25. Relations among MP moves and their inverses.

Proof. The proof for $A \leftrightarrow D^{-1}$ type, i.e., the proof for $A2 \leftrightarrow D1^{-1}$, $A3 \leftrightarrow D4^{-1}$, $A4 \leftrightarrow D3^{-1}$, are similar to that for $A1 \leftrightarrow D2^{-1}$ in figure 2.23 after adjusting the orientations of the two edges, see Figure 2.26.

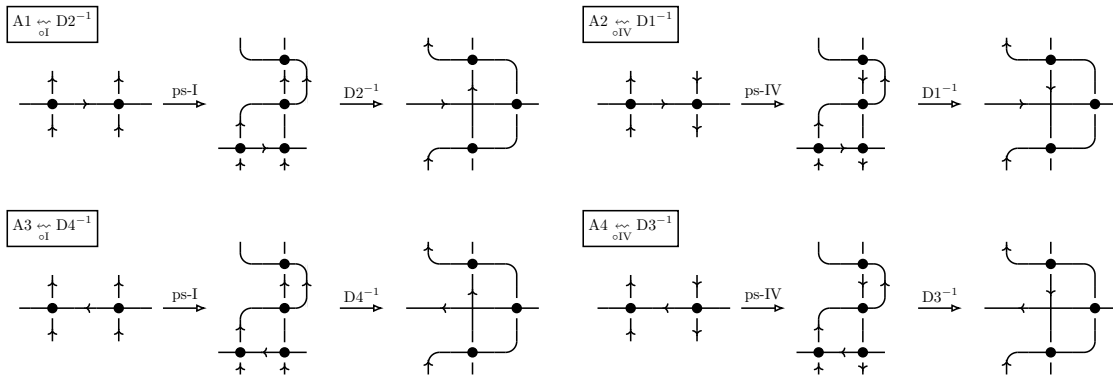


Figure 2.26. Proof of $A \leftrightarrow D^{-1}$ type.

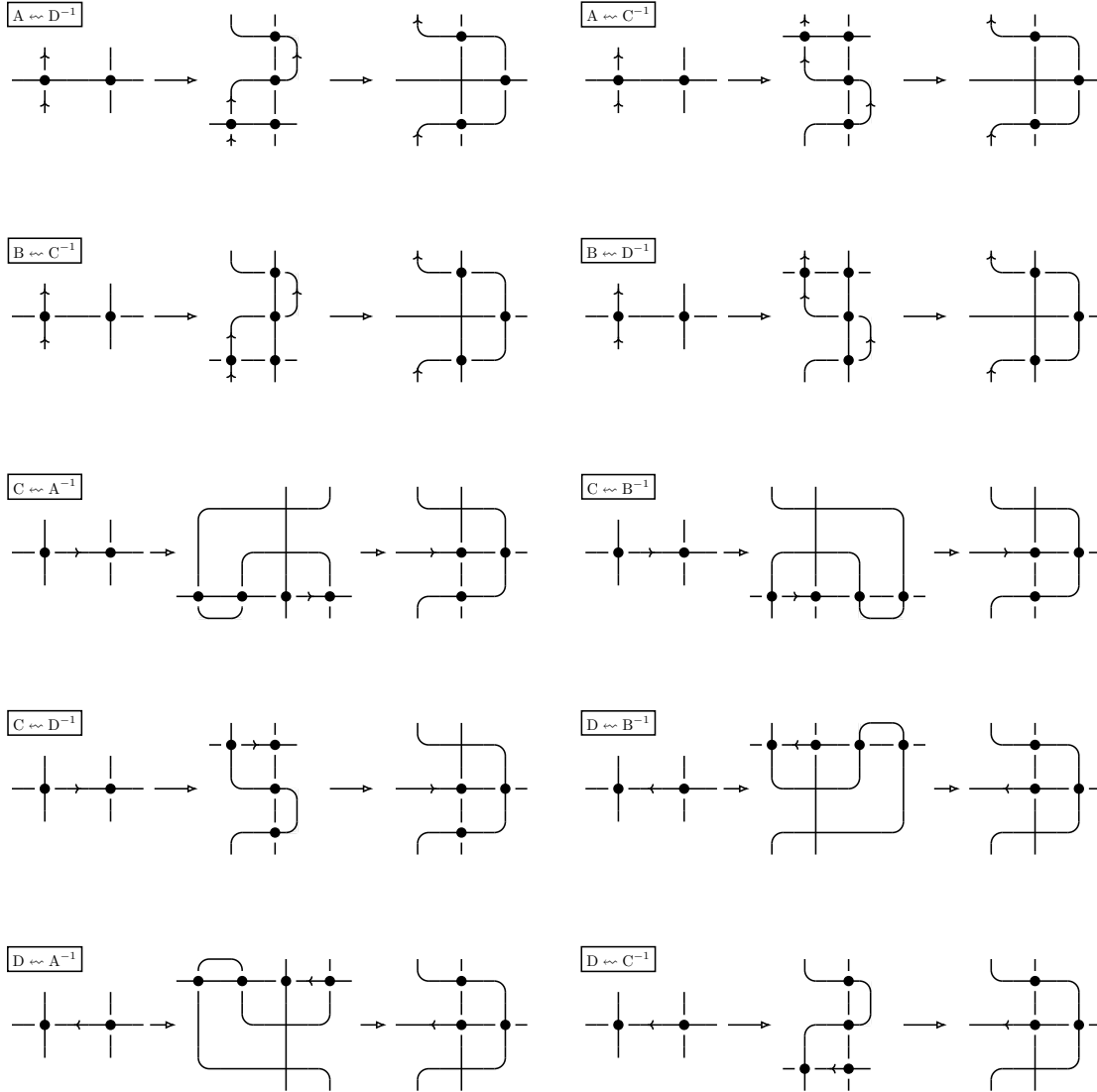


Figure 2.27. Proof of the diagrams in Figure 2.25.

Similarly, the proof of the types $A \rightsquigarrow C^{-1}$, $B \rightsquigarrow C^{-1}$, $B \rightsquigarrow D^{-1}$, $C \rightsquigarrow A^{-1}$, $C \rightsquigarrow B^{-1}$, $C \rightsquigarrow D^{-1}$, $D \rightsquigarrow A^{-1}$, $D \rightsquigarrow B^{-1}$, $D \rightsquigarrow C^{-1}$ are given as in Figure 2.27, where the types of the MP moves and the pure sliding moves follow the arrows in Figure 2.25. Thus we have the assertion. \square

Remark 2.3. In the diagram in Figure 2.25, there are lack of symmetries such that there are no arrow between moves of A-type and B-type. This is because of the asymmetry of the pure sliding moves and MP moves. If we consider including bumping moves (cf. [5, Figure 3.22, Figure 4.16]), the diagram becomes more symmetric.

Remark 2.4. We cannot derive any MP move or MP move inverse in the left diagram in Figure 2.25 from ones in the right diagram, and vice versa. This is because the number of positive true vertices minus the number of negative ones does not change under the pure sliding moves, and increases (resp. decreases) by one under the MP moves and the MP move inverses in the left (resp. right) diagram (cf. [5, Remark 3.5.4]).

Proof of Theorem 2.3. In Figure 2.25, observe that each pair of the MP moves at the same location in the left and right diagrams are inverses to each other, and the arrows at the same location in the left and right diagrams point in opposite directions. Recall that $A1 \rightsquigarrow_{\circ 1} D2^{-1}$ implies $A1^{-1} \rightsquigarrow_{1^{-1}\circ} D2$, which is also true for

other relations. Thus, we can transport each arrow of type $\overset{\leftarrow}{\circ}X$ being changed to the arrows of type $\overset{\leftarrow}{X^{-1}\circ}$ from the left diagram to the corresponding place in the right diagram, and vice versa. Consequently, all MP moves or their inverses in the same diagram are equivalent up to the pure sliding moves and their inverses, as shown in Figure 2.28. Here, $a \leftrightarrow b$ stands for $a \overset{\leftarrow}{\circ}X b$ and $a \overset{\rightsquigarrow}{Y^{-1}\circ} b$, or $a \overset{\leftarrow}{Y^{-1}\circ} b$ and $a \overset{\rightsquigarrow}{\circ}X b$, where each X and Y stands for one of ps-I – ps-IV.

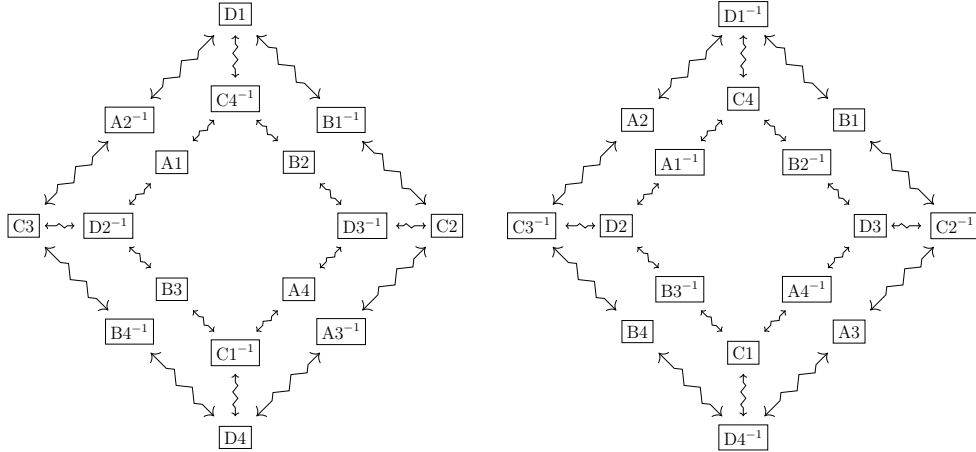


Figure 2.28. Relations among MP moves and their inverses up to the pure sliding moves and their inverses.

Observe that each type of the MP moves is either in the left or right diagram, and its inverse is in the other diagram. In particular, from $D2$ and $D2^{-1}$, we can obtain all MP moves and their inverses. This completes the proof of Theorem 2.3. \square

2.8. Local pure sliding moves and refinement of Theorem 2.3. By taking the above argument forward, we can refine Theorem 2.3 as follows. See the following pure sliding move which has already appeared in Figure 2.23.

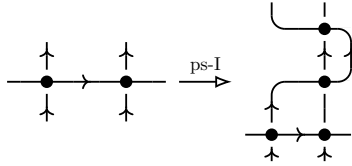


Figure 2.29. Local pure sliding move appearing in $A1 \leftrightarrow D2^{-1}$.

Recall that the two true vertices in the left picture enable us to check the condition (PS-I) locally as in Figure 2.24. Similarly, there are 40 pure sliding moves in the proof of Lemma 2.6 appearing as the first move in each sequence in Figure 2.27. We call these pure sliding moves *local pure sliding moves*.

Proposition 2.7. There is a set consisting of 18 local pure sliding moves such that each MP move is derived as a sequence of any MP move and 15 pure sliding moves in the set, and their inverses.

Proof. We initially select 18 arrows from the diagrams in Figure 2.25, as depicted in Figure 2.30. We can then convert each arrow of type $\overset{\leftarrow}{\circ}X$ into arrows of type $\overset{\leftarrow}{X^{-1}\circ}$ at corresponding locations in the other diagram, using a similar argument as in the proof of Theorem 2.3. Subsequently, we obtain oriented paths consisting of arrows, allowing us to travel from any MP move to another. Let's consider an arbitrary MP move, say $D2$ for example. We can remove 3 additional arrows, highlighted in gray in Figure 2.30, while maintaining connected paths from $D2$ or $D2^{-1}$. This process of removing 3 additional arrows can be applied to each MP move. Thus we have the assertion.

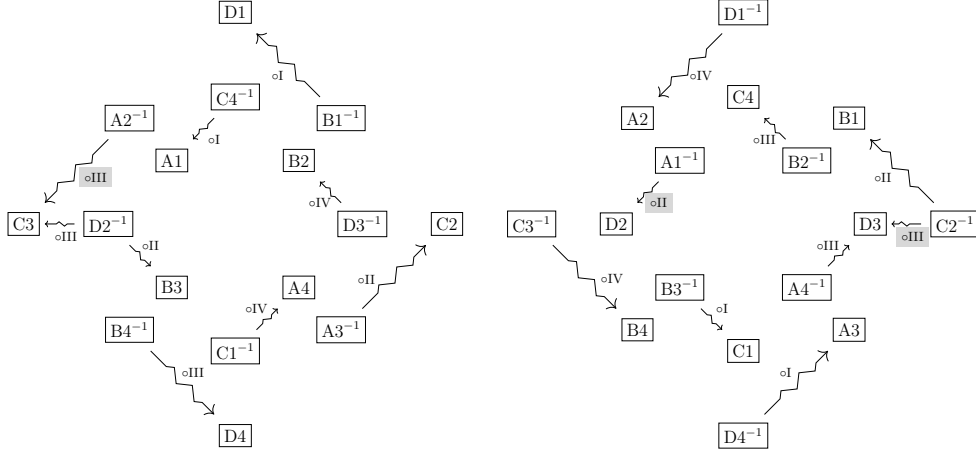


Figure 2.30. Paths by local pure sliding moves.

□

Corollary 2.8. Each MP move is derived as a sequence of the primary MP move and 15 local pure sliding moves, and their inverses.

Proof. Recall from Figure 2.22 that the primary MP move is equivalent to the MP move D2, which, together with Proposition 2.7, confirms the assertion. □

3. INTEGRAL NORMAL O-GRAPHS AND FRAMED 3-MANIFOLDS

In this section we follow the notation in [18].

3.1. Branched spines and framed 3-manifolds. In what follows we sometimes use metrics of 3-manifolds for convenience, while the results do not depend on them. Let M be a closed 3-manifold. A *framing* (v_1, v_2, v_3) of M is a trivialization of the tangent bundle TM such that $v_i \perp v_j$ for $i, j = 1, 2, 3$ and $i \neq j$. We assume that the orientation of M induced from the framing matches with the existing one. Two framed 3-manifolds (M, v_1, v_2, v_3) and (M', v'_1, v'_2, v'_3) are *equivalent* if there exists a diffeomorphism $h: M \rightarrow M'$ such that (h_*v_1, h_*v_2, h_*v_3) is homotopic through framings to (v'_1, v'_2, v'_3) . We denote by $\mathcal{M}_{\text{fram}}$ the set of equivalent classes of oriented framed 3-manifolds. Notice that we can obtain the third vector v_3 of a framing from v_1, v_2 and the orientation of M . Thus, we represent a framed 3-manifold as (M, v_1, v_2) specifying only the first two vectors v_1, v_2 .

Let P a closed branched spine representing a combed 3-manifold $(\widehat{M}(P), \widehat{v}_1(P))$. Observe that v_1 is perpendicular to P , thus $(\mathbb{R}\widehat{v}_1)^\perp$ is the “tangent bundle” of P , where tangency makes sense because P is branched. The Euler class $\mathcal{E} \in H^2(\widehat{M}; \mathbb{Z})$ of $(\mathbb{R}\widehat{v}_1)^\perp$ is the obstruction to the existence of a framing of M which extends v_1 , and is represented by the *Euler cochain* $c_P \in C^2(P; \mathbb{Z})$ defined in [5, Proposition 7.1]. We will explain the definition of the Euler cochain and its nature in Section 3.4 before we study framing explicitly.

Given a 1-cochain $x \in C^1(P; \mathbb{Z})$ satisfying $\delta x = c_P$, we can define the second vector $\widehat{v}_2(P, x)$ on $(\widehat{M}(P), \widehat{v}_1(P))$ as follows. We first define the second vector $v_2(P, x)$ on $M(P)$ near the 0-cells as in Figure 3.1.

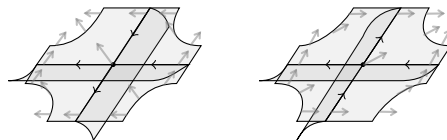


Figure 3.1. Second vector v_2 of framing near vertex of type + (left) and of type - (right).

Then we extend it over $S(P)$ so that the 1-cochain x defines the rotation number of $v_2(P, x)$ relative to the tangent vector of e having the canonical orientation coming from the branching of P . We extend it over 2-cells, where we can do this because of the boundary condition $\delta x = c_P$ ([5, Proposition 7.2.1]), and since $\pi_2(S^1) = 0$, the extension over the 2-cells are unique up to homotopy. Since $\pi_2(S^1) = \pi_3(S^1) = 0$, the second vector $v_2(P, x)$ defined on $M(P)$ extends uniquely to $\widehat{M}(P)$. Thus we get the unique framed 3-manifold $(\widehat{M}(P), \widehat{v}_1(P), \widehat{v}_2(P, x))$ up to equivalence. Conversely, every framed 3-manifold is obtained in this way [5, Proposition 7.2.4].

3.2. Integral normal o-graphs. An *integral normal o-graph* is a normal o-graph with an integer weight attached on each edge. Note that the correspondence of normal o-graphs and branched polyhedrons implies the correspondence of integral normal o-graphs and pairs (P, x) of a branched polyhedron P and its 1-cochain $x \in C^1(P; \mathbb{Z})$. A *framed integral normal o-graph* is an integral closed normal o-graph satisfying $\delta x = c_P$, which represents a framed 3-manifold. For example, see Figure 3.2 for framed integral normal o-graphs representing S^3 and the lens space $L(2, 1)$ with certain framings ⁸.

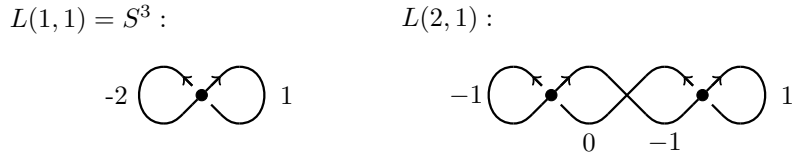


Figure 3.2. Framed integral normal o-graphs representing S^3 and $L(2, 1)$ with certain framings.

We consider three types of moves on framed integral normal o-graphs, the *integral 0-2 move* in Figure 3.3, the *integral MP-move* in Figure 3.4, and the *integral H-move* in Figure 3.5. Here, in Figure 3.4 the orientations of the non-oriented edges are arbitrary if they match before and after the move, and in Figure 3.4 and 3.5 if there are multiple weights on an edge after the move, the weights should be added in the additive group \mathbb{Z} . These moves do not change the framing of associated 3-manifolds [5, 18].

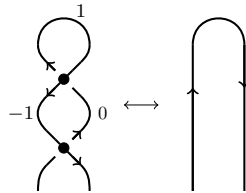


Figure 3.3. Integral 0-2 move.

⁸For S^3 it extends the combing induced by the Hopf fibration, and for the lens space $L(2, 1)$ it extends the canonical combing induced by its Seifert fibered structure [7].

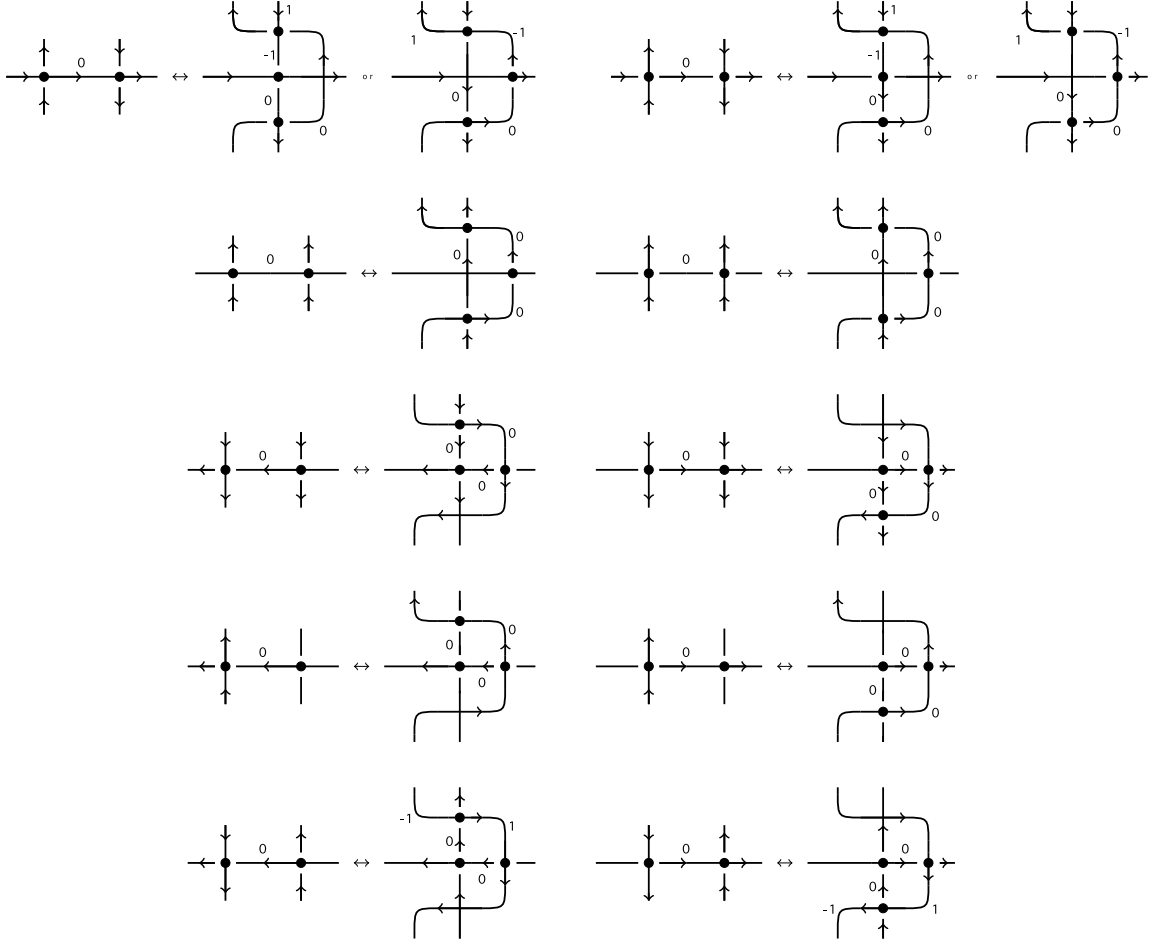


Figure 3.4. Integral MP-move. Orientation of each non-oriented edge is arbitrary if it matches before and after move.

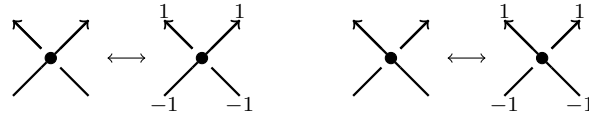


Figure 3.5. Integral H-move.

3.3. Framed normal o-graphs and framed 3-manifolds. The argument in the previous section shows that for each closed normal o-graph Γ and its 1-chain $x \in C^1(\Gamma; \mathbb{Z})$ such that $\delta x = c_P$ we have a framed 3-manifold $\Phi_{\text{fram}}(\Gamma, x)$, and each equivalent class of framed 3-manifolds is obtained in this way. In fact, $\Phi_{\text{fram}}(\Gamma, x)$ depends only on $(\Gamma, [x]_2)$, where $[x]_2 \in C^1(\Gamma, \mathbb{Z}_2)$ is the projection of $x \in C^1(\Gamma, \mathbb{Z})$ ([5, Theorem]).

A *framed normal o-graph* [5] is the image $(\Gamma, [x]_2)$ of a framed integral normal o-graph (Γ, x) by the projection on the second factor. We denote by $\mathcal{G}_{\text{fram}}$ the set of framed normal o-graphs, and define the *framed 0-2 move*, the *framed MP-move*, and the *framed H-move* on $\mathcal{G}_{\text{fram}}$ as the projections of the corresponding integral moves on integral normal o-graphs. With these conventions, we have a surjective map

$$\Phi_{\text{fram}} : \mathcal{G}_{\text{fram}} \rightarrow \mathcal{M}_{\text{fram}}.$$

Proposition 3.1 (Benedetti-Petronio [5, Theorem 1.4.3]). The equivalence relation defined by Φ_{fram} is generated by the framed 0-2 move, the framed MP moves, and the framed H-move.

3.4. Euler cochain c_P . In the next section we will define pure sliding moves on framed normal o-graphs, where the well-definedness (Proposition 3.2) requires arguments including the nature of the Euler cochain c_P . For this reason we explain c_P in this section, see [5] for more details.

Let P be a branched polyhedron. The Euler cochain of P is given by

$$c_P = - \sum_i (1 - n_i/2) \hat{\Delta}_i \in C^2(P; \mathbb{Z}),$$

where $\hat{\Delta}_i \in C^2(P; \mathbb{Z})$ is the dual of a connected component Δ_i (2-cells) of $D(P)$, and the dots n_i is the total number of solid dots as in Figure 3.6 on the boundary of Δ_i .

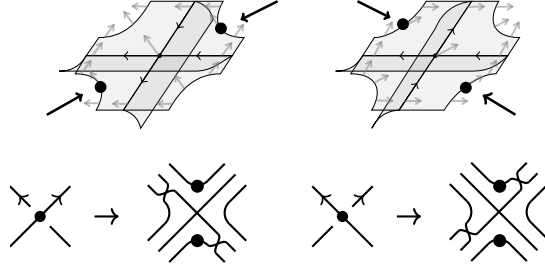


Figure 3.6. Solid dots on boundary of Δ_i .

Let v be the vector field on $S(P)$ tangent to P , defined around $V(P)$ by the gray arrows in Figure 3.1 (and in the top of Figure 3.6), while v outside $V(P)$ is defined to not be tangent to $S(P)$. The Euler cochain c_P is constructed as the obstruction to extending v to P as follows: In Figure 3.6, the solid dots on Δ_i indicate points where v is tangent to $\partial\Delta_i$. When counting the rotation number of v on $\partial\Delta_i$ relative to the tangent vector of $\partial\Delta_i$, each time we pass through a dot, the vector v rotates by $-1/2$. The total rotation number is thus $-n_i/2$. Consequently, the vector field v extends to 2-cells if and only if $-n_i/2 = -1$ for each i , which is equivalent to $c_P = 0$. In general, for $x \in C^1(P; \mathbb{Z})$, let v_x be the vector field on $S(P)$ obtained by rotating v using x as described in Section 3.1. Then, $\delta x - c_P$ represents the obstruction to extending v_x to 2-cells.

3.5. Integral pure sliding moves on integral normal o-graphs. We introduce the *integral pure sliding moves* I – IV as in Figure 3.7, where we can perform them only when the underlying normal o-graphs satisfy the conditions (PS-I)–(PS-IV), respectively.

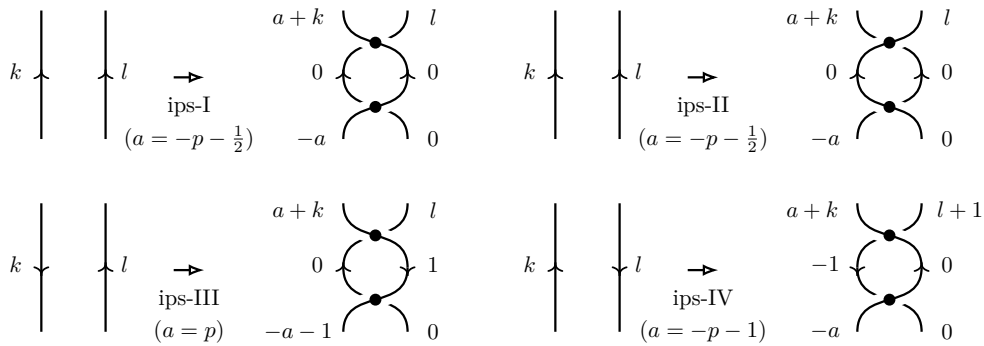


Figure 3.7. Integral pure sliding move ips-I – ips-IV.

Here, k and l represent integer weights assigned to parts of edges. If there are multiple weights on an edge, the integer weight of the edge is the sum of these weights (for instance, the case when two open edges above are parts of one edge). Additionally, $p \in \mathbb{Z}/2$ is an integer or half-integer defined as follows.

Let P be a branched spine of M , and $x \in C^1(P; \mathbb{Z})$ be a cochain representing a framing of M . Consider the 2-cell Δ on which we perform the pure sliding move. The boundary $\partial\Delta$ is oriented as usual, traveling along edges of P (potentially visiting one edge multiple times). We can then determine the rotation number of the second vector v_2 of framing on $\partial\Delta$ using $x \in C^1(P; \mathbb{Z})$, as depicted in the left image of Figure 3.8.

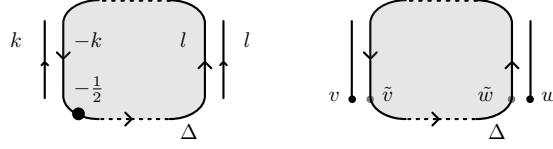


Figure 3.8. How we count rotation number on Δ (left) and points \tilde{v} and \tilde{w} on $\partial\Delta$ (right).

Namely, when $\partial\Delta$ passes along an edge e in the direction induced by Δ , if e is oriented in the same direction as $\partial\Delta$ proceeds, then the rotation number on that part is $x(e)$; otherwise, it is $-x(e)$. When $\partial\Delta$ passes along a vertex, if there is a solid dot as shown in Figure 3.6, then we count $-1/2$.

Refer to the defining picture of ips moves in Figure 3.7. Let e_1 and e_2 be the left and right open edges, respectively, on which we perform an ips move. We can assume that on the edges where e_1 and e_2 reside, the second vector v_2 of the framing rotates k and l times inside e_1 and e_2 , respectively, while outside it goes transversely to the edge from left to right following the edge's orientation (the opposite direction of the branching). Then, p represents the rotation number of v_2 on $\partial\Delta$ from the bottom of e_1 (positioned as shown in Figure 3.7) to the bottom of e_2 .

We can calculate p as follows. If the bottoms of e_1 and e_2 are connected without a vertex, then $p = 0$. If there are vertices, let v and w be the vertices (potentially the same vertex) that we encounter when we reach the bottom of e_1 and e_2 , respectively, see the right image of Figure 3.8. Let \tilde{v} and \tilde{w} be the points (again, they could be the same point) on $\partial\Delta$ attached to v and w , respectively, at the bottom of the sliding region (the pre-image is not globally unique). Then, p is the rotation number of v_2 on $\partial\Delta$ from \tilde{v} to \tilde{w} , where if there is a solid dot at \tilde{v} or \tilde{w} , we count $-1/2$ for each of them.

Proposition 3.2. Let Γ and Γ' be two framed integral normal o-graphs which are related by the integral pure sliding moves. Then the framed 3-manifolds induced by Γ and Γ' are equivalent.

Proof. We prove the assertion for ips-I. For the other moves the proof is similar.

Let (Γ, x) be a framed integral normal o-graph and (Γ', x') be the integral normal o-graph obtained from (Γ, x) by ips-I. Let Δ be the 2-cell on which we perform ips-I. We first divide Δ into five disks Δ_1 – Δ_5 as the left picture in Figure 3.9. Then we arrange the second vector v_2 of the framing on Δ by homotopy which is the identity on the boundary, as in the right picture, where the integer of each edge represents the rotation number relative to the orientation of the boundary of the disks, and each white dot represents the tangency points which has the rotation number $-1/2$. We can do this because on each disk the total rotation number on the boundary is -1 : for Δ_2, Δ_3 , and Δ_4 , this follows by straightforward calculation; for Δ_5 , it follows from the definition of $a = -p - 1/2$; and for Δ_1 , it follows from the definition of a and the equation derived from the initial condition that the rotation number on $\delta\Delta$ is -1 .

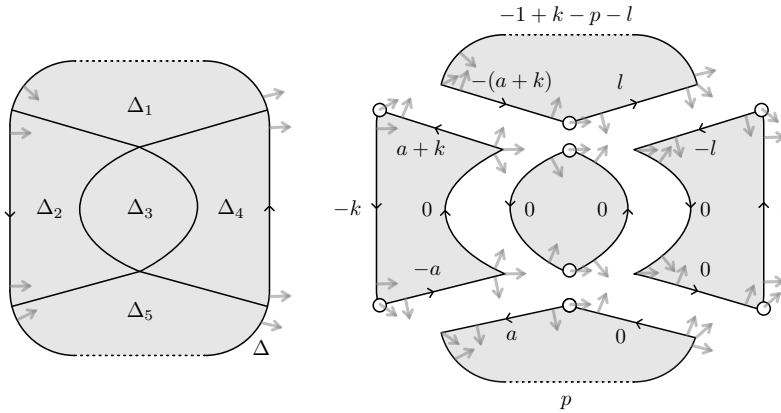


Figure 3.9. Decomposition of Δ (left) and second vector v_2 of framing on Δ (right).

Let M be the framed 3-manifold obtained by (Γ, x) . Near the sliding region, we consider a planar figure, and we assume that the branched spine is almost horizontal so that the second vector v_2 of the framing is

obtained by the pullback of the projection to the horizontal plane. Under this setting, we can pull back v_2 as depicted in the right picture in Figure 3.9, thus defining the framing of M near the sliding region. Note that this framing is a representative for both the homotopy classes of framings obtained from (Γ, x) and (Γ', x') . Thus we have the assertion. \square

Remark 3.1. In [5, Section 7.3], the authors demonstrated results similar to Proposition 3.2, showing that the framed 0-2 move and the framed MP move do not alter the framing of closed 3-manifolds. They illustrated local framing changes near the sliding regions explicitly by projecting them onto a plane [5, Figure 7.7–7.9]. This is feasible because they can assume the cochain $x \in C^1(P, \mathbb{Z})$ affects regions far from the sliding regions, allowing to take an explicit framing near sliding regions. However, in our case, this approach is not applicable in Figure 3.9 because the framing near the sliding region depends on the framing on the boundary of Δ_1 and Δ_5 out of the sliding region.

3.6. Main results for framed 3-manifolds. We define the primary integral MP move as follows.

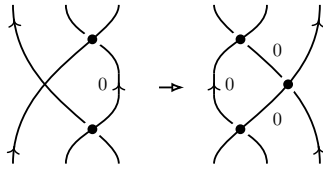


Figure 3.10. Primary integral MP move.

Theorem 3.3. Each of the 16 integral MP move in Figure 3.4 is derived as a sequence of the primary integral MP move, the integral pure sliding moves, the integral H-move and their inverses.

Proof of Theorem 3.3. The proof follows a similar path to the proof of Theorem 2.3, once integer weights are attached. The detailed proof is left to the readers. \square

By taking modulo 2 on each integer weight, we have the following.

Corollary 3.4. Each of the 16 framed MP move is derived as a sequence of the primary framed MP move, the framed pure sliding moves, the framed H-move and their inverses.

Note that the integral 0-2 move is an integral pure sliding move. By Proposition 3.1, Proposition 3.2 and Theorem 3.4, we have the following representation of framed 3-manifolds.

Corollary 3.5. The equivalence relation defined by the surjective map $\Phi_{\text{fram}}: \mathcal{G}_{\text{fram}} \rightarrow \mathcal{M}_{\text{fram}}$ is generated by the primary framed MP move, the framed pure sliding moves and the framed H-move.

3.7. Local integral pure sliding moves and refinement of Theorem 3.3. In this section we give a refinement of Theorem 3.3, which generalizes Proposition 2.7. The integral pure sliding moves are local in the sense that the normal o-graph does not change outside the sliding region. However, they are not local in the sense that we need global information about the 2-cells to perform the moves (as with pure sliding moves on normal o-graphs), and moreover, the resulting cochain also depends on the global information of the original cochain, as noted in Remark 3.1.

We define *local integral pure sliding moves* by attaching integer weights to the 40 local pure sliding moves defined in Section 2.8.

Corollary 3.6. Each integral MP move is derived as a sequence of the primary integral MP move and 15 local integral pure sliding moves and their inverses.

Proof. The proof is similar to that of Proposition 2.7. \square

4. SPIN NORMAL O-GRAPHS AND SPIN 3-MANIFOLDS

A spin structure of a 3-manifold with a standard spine P can be thought of as a homotopy class of framing over the 1-skeleton that extends over the 2-skeleton. Let Γ be a closed normal o-graph. Spin structures on $M(\Gamma)$ correspond bijectively to cochains $z \in C^1(P(\Gamma), \mathbb{Z}_2)$ such that $\partial z = (c_p)_2 \in C^2(P(\Gamma), \mathbb{Z}_2)$, where two cochains are viewed as equivalent if they differ by a 1-coboundary [5, Proposition 7.4.2]. A *spin normal*

o-graphs is a pair (Γ, y) of a normal *o-graph* Γ and $y \in C^1(\Gamma, \mathbb{Z}_2)$ such that $\partial y = (c_p)_2$. We denote by $\mathcal{G}_{\text{spin}}$ the set of spin normal *o-graphs*. Thus we have a surjective map

$$\Phi_{\text{spin}} : \mathcal{G}_{\text{spin}} \rightarrow \mathcal{M}_{\text{spin}}.$$

We define the *framed 0-2 move*, the *framed MP moves*, the *framed H-move* on $\mathcal{G}_{\text{spin}}$ in a similar way to these on $\mathcal{G}_{\text{fram}}$.

Proposition 4.1 (Benedetti-Petronio [5, Theorem 1.4.4]). The equivalence relation defined by Φ_{spin} is generated by the framed 0-2 move, the framed MP moves, the framed H-moves, and the *framed CP move* defined in [5, Figure 1.9].

We define framed pure sliding moves on $\mathcal{G}_{\text{spin}}$ in a similar way to these on $\mathcal{G}_{\text{fram}}$.

Proposition 4.2. Let (Γ, y) and (Γ', y') be two spin normal *o-graphs* which are related by the framed pure sliding moves. Then the induced spin 3-manifolds are equivalent.

Proof. Using the similar assumption of the proof of Proposition 3.2, we can represent each spin structure near the sliding region by a framing on Δ whose first vector on the boundary of the disks Δ_1 – Δ_5 is $v_1 = v(P)$ (cf. [5, Lemma 7.4.1]) and the second vector on the boundary of the disks Δ_1 – Δ_5 is given by the rotation number on each edge as in Figure 3.9, where the integer weights are considered in \mathbb{Z}_2 . This framing is a representative for the spin structures obtained from (Γ, y) and (Γ', y') . Thus we have the assertion. \square

Corollary 4.3. The equivalence relation defined by the surjective map $\Phi_{\text{spin}} : \mathcal{G} \rightarrow \mathcal{M}_{\text{spin}}$ is generated by the primary framed MP move, the framed pure sliding move, the framed H-move and the framed CP move.

Proof. The assertion follows immediately from Corollary 3.4, Propositions 4.1 and 4.2. \square

A. SYMMETRY OF MOVES

In this section, we investigate the symmetries of the MP moves. In what follows, we assume, for simplicity, that the normal *o-graph* Γ is closed, although the argument applies to normal *o-graphs* in general. Let $P(\Gamma)$ be the branched polyhedron represented by Γ , as explained in Section 2.2. Recall from Section 2.3 the equivalent class of a combed 3-manifold $(\widehat{M}(\Gamma), \widehat{v}(\Gamma))$ obtained from the branched spine $P(\Gamma)$. For brevity, we will denote it by $(M(\Gamma), v(\Gamma))$, omitting the hats. We may occasionally use the same notation for a representative of the equivalent class.

Let Γ^* , $\overrightarrow{\Gamma}$, and Γ^\times be the normal *o-graphs* obtained from a normal *o-graph* Γ by reflecting its diagram, reversing its orientation, and changing the sign of every crossing, respectively. Note that each of these operations is involutive.

For a combed 3-manifold $(M(\Gamma), v(\Gamma))$, let $(M^{\text{op}}(\Gamma), v^{\text{op}}(\Gamma))$ be the equivalent class of combed 3-manifolds defined by the image of $(M(\Gamma), v(\Gamma))$ under an orientation-reversing diffeomorphism. For a combing v of a 3-manifold we denote by $-v$ the combing obtained by multiplying (-1) to v at each point.

Proposition A.1. We have $(M(\overrightarrow{\Gamma^*}), v(\overrightarrow{\Gamma^*})) = (M^{\text{op}}(\Gamma), v^{\text{op}}(\Gamma))$ and $(M(\Gamma^\times), v(\Gamma^\times)) = (M^{\text{op}}(\Gamma), -v^{\text{op}}(\Gamma))$.

Proof. We first consider Γ^\times . Recall from Section 2.2 the construction of the branched spine $P(\Gamma)$ from a normal *o-graph* Γ , and recall from Figure 2.6 the correspondence between a crossing of Γ and a neighborhood (butterfly) of the corresponding true vertex in $P(\Gamma)$. When we change the sign of a crossing, the corresponding butterfly is reflected in \mathbb{R}^3 by the xy -plane on which the four horizontal 2-cells in the butterfly are placed, see Figure A.1.

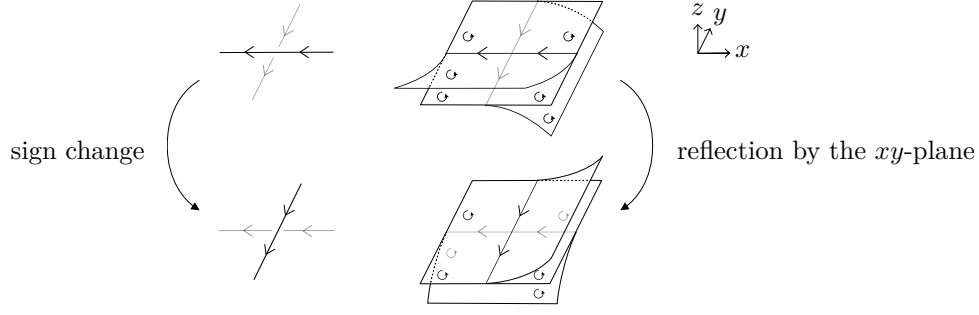


Figure A.1. Sign change of normal o-graph and corresponding butterfly.

This correspondence induces the orientation-reversing diffeomorphism $f: (x, y, z) \mapsto (x, y, -z)$ between neighborhoods of butterflies in $M(\Gamma)$ and $M(\Gamma^\times)$, and we can extend it to whole 3-manifolds. Note that the push-forward $f_*(v(\Gamma))$ of the combing in $M(\Gamma)$ goes to $-z$ direction which is opposite to the combing of $M(\Gamma^\times)$ that goes to z direction. Consequently we have $(M(\Gamma^\times), v(\Gamma^\times)) = (f(M(\Gamma)), -f_*(v(\Gamma))) = (M^{\text{op}}(\Gamma), -v^{\text{op}}(\Gamma))$.

We then consider $(\vec{\Gamma}^\times)^\times$, performing all 3 involutions. When we perform them around a crossing of a Γ , the corresponding butterfly in $P(\Gamma)$ is flipped, i.e., rotated π degrees around the line in the xy -plane which we use when we reflect the diagram of the crossing. Here, the orientation of edges of the normal o-graph is reversed because the orientation of 2-cells is reversed after we flip it, according to the assumption for constructing the diagram that the orientation of the 2-cell should be compatible with that of the xy -plane, see Figure A.2.

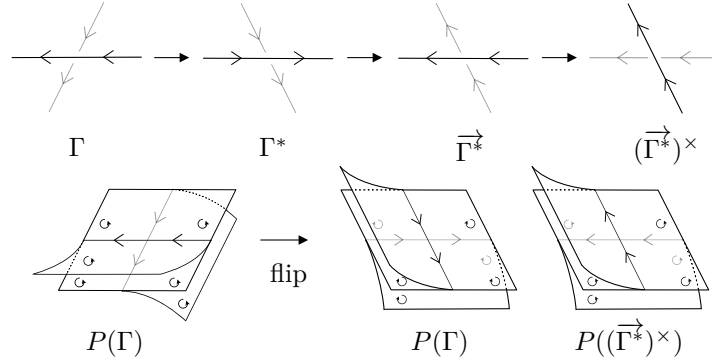


Figure A.2. Performing all involutions on normal o-graph and resulting butterfly.

This flip is extended to an orientation-preserving diffeomorphism of whole 3-manifolds, and the combing is reversed because the orientation of the 2-cell is reversed. Thus we have $(M((\vec{\Gamma}^\times)^\times), v((\vec{\Gamma}^\times)^\times)) = (M(\Gamma), -v(\Gamma))$.

For $\vec{\Gamma}^\leftarrow = ((\vec{\Gamma}^\times)^\times)^\times$, the above two cases imply that $(M(\vec{\Gamma}^\leftarrow), v(\vec{\Gamma}^\leftarrow)) = (M^{\text{op}}(\Gamma), v^{\text{op}}(\Gamma))$, see Figure A.3, which completes the proof.

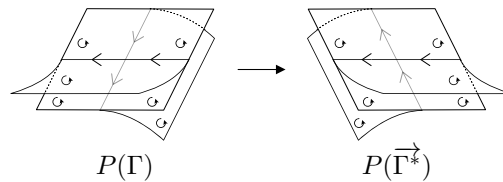


Figure A.3. Butterflies in $P(\Gamma)$ and $P(\vec{\Gamma}^\leftarrow)$.

□

We study the behavior of the 16 MP moves and pure sliding moves under the involutions $\overleftarrow{\circ}^*$ (reflect and reverse the orientation) and \times (change the sign of each crossing). Tables 1 and 2 show the results of moves by the involutions. For example, if a normal o-graph Γ_2 is obtained from another normal o-graph Γ_1 by A1 on vertices v_1, v_2 of Γ_1 , then $\overleftarrow{\Gamma}_2^*$ is obtained from $\overleftarrow{\Gamma}_1^*$ by A3 on the image of vertices v_1, v_2 by $\overleftarrow{\circ}^*$.

	A1	A2	A3	A4	B1	B2	B3	B4	C1	C2	C3	C4	D1	D2	D3	D4
reflect * & reverse $\overleftarrow{\circ}$	A3	A4	A1	A2	B3	B4	B1	B2	D1	D2	D3	D4	C1	C2	C3	C4
sign change \times	B1	B2	B3	B4	A1	A2	A3	A4	D4	D2	D3	D1	C4	C2	C3	C1

Table 1. Symmetries of MP moves.

	ps-I	ps-II	ps-III	ps-IV
reflect * & reverse $\overleftarrow{\circ}$	ps-I	ps-II	ps-III	ps-IV
sign change \times	ps-II	ps-I	ps-III	ps-IV

Table 2. Symmetries of pure sliding moves.

By using the above argument, we can simplify the proof of Lemma 2.6. One can check that the right diagram in Figure 2.25 is equal to the image of the left diagram by $\overleftarrow{\circ}^*$, and also the image by \times .

In Proposition 2.7, we can chose a set of 18 local pure sliding moves consisting of 9 local pure sliding moves and their image by $\overleftarrow{\circ}^*$, or their image by \times , which is for example the 9 arrow in the left diagram in Figure 2.28.

B. CYCLIC MOVES

In this section we study cyclic moves as we introduced in the introduction. Note that the MP moves A2, A4, B2, B4, C3, D3 are cyclic, and the others are non-cyclic. For the pure sliding moves, ps-I and ps-II are non-cyclic, and ps-III and ps-IV are cyclic. The inverse of a (non-) cyclic move will also be referred to as a (non) cyclic move.

Proposition B.1. Each non-cyclic MP move is derived as sequence of the primary MP move (which is non-cyclic), the non-cyclic pure sliding moves, and their inverses. Any cyclic MP move cannot be derived as a sequence of non-cyclic moves. Especially, each cyclic MP move must include a cyclic pure sliding moves in a sequence of the primary MP move, the pure sliding moves and their inverses representing it.

Proof. Refer to Figure B.1, where we highlight the cyclic moves in the diagram from Figure 2.25, depicting the relationships of the MP moves. (Actually, the right diagram is unnecessary since it is the image of the involutions $\overleftarrow{\circ}^*$ or \times , as explained in the previous section, and these involution keep the cyclic property.)

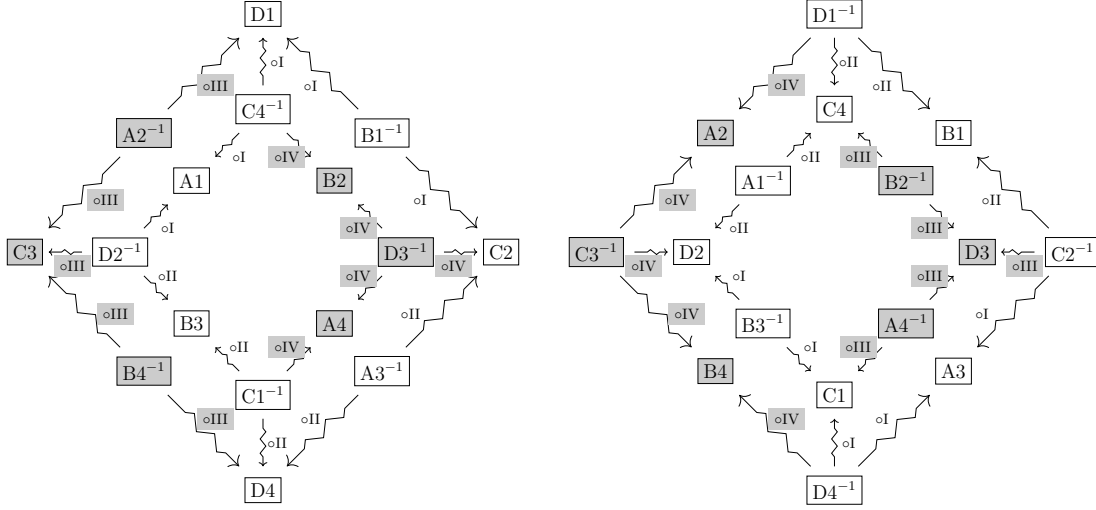


Figure B.1. Cyclic MP moves and cyclic pure sliding moves in diagram in Figure 2.25.

Remember that the primary MP move is equivalent to the MP move D2. Figure B.1 illustrates that each non-cyclic MP move is a sequence of the primary MP move, the non-cyclic pure sliding moves, and their inverses.

By using the invariant Z defined for integral normal o-graphs in [18] for non-involutive Hopf algebras, we can show that any cyclic MP move cannot be derived as a sequence of non-cyclic moves. To be more precise, we apply Z to a normal o-graph Γ treating it as an integral normal o-graph $\Gamma(0)$ with a zero weight on each edge. To avoid confusion we denote the resulting map on normal o-graphs by Z^0 , and we compare the value $Z^0(\Gamma) = Z(\Gamma(0))$ and $Z^0(\Gamma') = Z(\Gamma'(0))$ when Γ and Γ' are related by a (non-) cyclic move. Here, strictly speaking, we consider *normal o-tangles* treating Z as a functor from the category of integral normal o-tangles (cf. [18, Remark 3.1]), to compare the values of Z^0 locally around the move. While the invariant Z^0 remains unchanged under non-cyclic moves, it is not invariant under cyclic moves for non-involutive Hopf algebras. In fact, it is not difficult to observe that Z^0 is invariant under a cyclic move if and only if the Hopf algebra is involutive, see the proofs of [17, Theorem 5.1] and [18, Theorem 3.3], see also Remark B.1 below. If a cyclic move were a sequence of non-cyclic moves, it would imply that the cyclic move does not change the value of Z^0 , leading to a contradiction. \square

We also classify integral moves as either cyclic or non-cyclic based on the underlying move for normal o-graphs.

Corollary B.2. Each integral non-cyclic MP move is derived as sequence of the integral primary MP move, the integral non-cyclic pure sliding moves, and their inverses. Any integral cyclic MP move cannot be derived as a sequence of integral non-cyclic moves.

Proof. The proof for the former part is similar to that of the former part of Proposition B.1, once integer weights are attached. For the latter part, we can extend the arguments for the latter part of Proposition B.1 to integral normal o-graphs and integral moves by considering the underlying normal o-graphs. \square

Remark B.1. In [17], we introduced an invariant Z of combed 3-manifolds using normal o-graphs and involutive Hopf algebras, which is essentially equivalent to Z^0 discussed in the proof of Proposition B.1. To avoid confusion with Z introduced in [18], we will denote the former as Z^0 in the following discussion. In [18], we extended Z^0 to integral normal o-graphs and any Hopf algebra to define Z . In this extended formulation, the integer weight i on an edge of an integral normal o-graph affects as S^{2i} with the antipode S of the Hopf algebra. Thus, when we work with an involutive Hopf algebra, the invariant Z for integral normal o-graphs reduces to Z^0 for normal o-graphs by applying it to underlying normal o-graphs, resulting in an invariant of combed 3-manifolds. If the involutive Hopf algebra is in addition unimodular and counimodular, then Z becomes invariant under the CP move and gives a topological invariant of 3-manifolds.

For non-involutory Hopf algebras, Z^0 fails to be an invariant for combed 3-manifolds because it is not invariant under cyclic moves, although it remains invariant under non-cyclic moves. To address this, in [18], we introduced integral normal o-graphs and extended Z from Z^0 ensuring its invariance under integral cyclic moves. This extension results in an invariant for framed 3-manifolds.

Note that integral cyclic moves have non-trivial integer weights as illustrated in Figure 3.4, which help reconcile the disparities of the values of Z^0 before and after cyclic moves. On the other hand, integral non-cyclic moves have everywhere zero weights and thus Z is compatible with Z^0 , i.e., $Z((\Gamma, x)) = Z((\Gamma, 0)) = Z^0(\Gamma)$ locally around non-cyclic moves, tearing Z as a functor from integral normal o-tangles as mentioned in the proof of Proposition B.1.

In the above argument, the obstruction preventing Z^0 for a non-involutory Hopf algebra from becoming an invariant of combed 3-manifolds (or topological 3-manifolds) is the invariance under cyclic moves. From the viewpoint of Proposition B.1, the obstruction lies essentially in the cyclic pure sliding moves, specifically ps-III and ps-IV. We can strengthen this statement further. As depicted in Figure B.1, each cyclic MP move is a sequence consisting of a non-cyclic MP move (or its inverse) and a cyclic pure sliding move (or its inverse). Consequently, Z^0 is invariant under a cyclic MP move if and only if Z^0 is invariant under cyclic pure sliding moves. A straight forward calculation shows that Z^0 is invariant under ps-III (or equivalently ps-IV) if and only if the Hopf algebra is involutory. To summarize, Z^0 is invariant under cyclic moves if and only if the Hopf algebra is involutory.

In other words, the invariant Z for a non-involutory Hopf algebra captures framings of 3-manifolds (at least locally; if not, the Hopf algebra should be involutory), and algebraic equations in the non-involutory Hopf algebra coming from the geometrical equivalence relation (homotopy) of framings via Z are reduced to algebraic properties of the square of the antipode. Specifically, if $S^2 = 1$, the equations become trivial. Further study of the relationship between framings and the properties of S^2 would be interesting.

REFERENCES

- [1] J. E. Andersen and R. Kashaev, *A TQFT from quantum Teichmüller theory*, *Comm. Math. Phys.* **330** (2014), no. 3, 887–934, DOI 10.1007/s00220-014-2073-2. MR3227503
- [2] S. Baseilhac and R. Benedetti, *Quantum hyperbolic invariants of 3-manifolds with $\mathrm{PSL}(2, \mathbb{C})$ -characters*, *Topology* **43** (2004), no. 6, 1373–1423, DOI 10.1016/j.top.2004.02.001. MR2081430
- [3] ———, *Classical and quantum dilogarithmic invariants of flat $\mathrm{PSL}(2, \mathbb{C})$ -bundles over 3-manifolds*, *Geom. Topol.* **9** (2005), 493–569, DOI 10.2140/gt.2005.9.493. MR2140989
- [4] ———, *Non ambiguous structures on 3-manifolds and quantum symmetry defects*, *Quantum Topol.* **8** (2017), no. 4, 749–846, DOI 10.4171/QT/101. MR3737277
- [5] R. Benedetti and C. Petronio, *Branched standard spines of 3-manifolds*, *Lecture Notes in Mathematics*, vol. 1653, Springer-Verlag, Berlin, 1997.
- [6] V. V. Fok and L. O. Chekhov, *Quantum Teichmüller spaces*, *Teoret. Mat. Fiz.* **120** (1999), no. 3, 511–528, DOI 10.1007/BF02557246 (Russian, with Russian summary); English transl., *Theoret. and Math. Phys.* **120** (1999), no. 3, 1245–1259. MR1737362
- [7] M. Endoh and I. Ishii, *A new complexity for 3-manifolds*, *Japan. J. Math. (N.S.)* **31** (2005), no. 1, 131–156.
- [8] L. D. Faddeev, *Discrete Heisenberg-Weyl group and modular group*, *Lett. Math. Phys.* **34** (1995), no. 3, 249–254, DOI 10.1007/BF01872779. MR1345554
- [9] V. Fock and A. Goncharov, *Moduli spaces of local systems and higher Teichmüller theory*, *Publ. Math. Inst. Hautes Études Sci.* **103** (2006), 1–211, DOI 10.1007/s10240-006-0039-4. MR2233852
- [10] V. V. Fock and A. B. Goncharov, *The quantum dilogarithm and representations of quantum cluster varieties*, *Invent. Math.* **175** (2009), no. 2, 223–286, DOI 10.1007/s00222-008-0149-3. MR2470108
- [11] I. Ishii, *Moves for flow-spines and topological invariants of 3-manifolds*, *Tokyo J. Math.* **15** (1992), no. 2, 297–312.
- [12] R. M. Kashaev, *The Heisenberg double and the pentagon relation*, *Algebra i Analiz* **8** (1996), no. 4, 63–74; English transl., *St. Petersburg Math. J.* **8** (1997), no. 4, 585–592.
- [13] ———, *Quantization of Teichmüller spaces and the quantum dilogarithm*, *Lett. Math. Phys.* **43** (1998), no. 2, 105–115, DOI 10.1023/A:1007460128279. MR1607296
- [14] A. N. Kirillov and N. Yu. Reshetikhin, *Representations of the algebra $U_q(\mathfrak{sl}(2))$, q -orthogonal polynomials and invariants of links*, *Infinite-dimensional Lie algebras and groups (Luminy-Marseille, 1988)*.
- [15] R. J. Lawrence, *A universal link invariant*, *The interface of mathematics and particle physics (Oxford, 1988)*, 151–156, *Inst. Math. Appl. Conf. Ser. New Ser.*, **24**, Oxford Univ. Press, New York, 1990.
- [16] S. Matveev, *Algorithmic topology and classification of 3-manifolds*, 2nd ed., *Algorithms and Computation in Mathematics*, vol. 9, Springer, Berlin, 2007.
- [17] S. M. Mihalache, S. Suzuki, and Y. Terashima, *The Heisenberg double of involutory Hopf algebras and invariants of closed 3-manifolds*, *Algebr. Geom. Topol.* to appear. preprint (2021), arXiv:math.GT/2104.03037.

- [18] ———, *Quantum invariants of framed 3-manifolds based on ideal triangulations*. preprint (2022), arXiv:math.GT/2209.07378.
- [19] T. Ohtsuki, *Colored ribbon Hopf algebras and universal invariants of framed links*, *J. Knot Theory Ramifications* **2** (1993), no. 2, 211–232.
- [20] N. Yu. Reshetikhin and V. G. Turaev, *Ribbon graphs and their invariants derived from quantum groups*, *Comm. Math. Phys.* **127** (1990), no. 1, 1–26.
- [21] N. Reshetikhin and V. G. Turaev, *Invariants of 3-manifolds via link polynomials and quantum groups*, *Invent. Math.* **103** (1991), no. 3, 547–597.
- [22] S. Suzuki, *The universal quantum invariant and colored ideal triangulations*, *Algebr. Geom. Topol.* **18** (2018), no. 6, 3363–3402.
- [23] ———, *Quantum invariants based on ideal triangulations*, *RIMS Kôkyûroku* **2263** (2023), 48–67.
- [24] V. G. Turaev and O. Ya. Viro, *State sum invariants of 3-manifolds and quantum 6j-symbols*, *Topology* **31** (1992), no. 4, 865–902, DOI 10.1016/0040-9383(92)90015-A. MR1191386
- [25] E. Witten, *Quantum field theory and the Jones polynomial*, *Comm. Math. Phys.* **121** (1989), no. 3, 351–399.

MIZUHO RESEARCH & TECHNOLOGIES, LTD., 5-16-6, HAKUSAN, BUNKYO-KU, TOKYO 112-0001, JAPAN
Email address: kohei.muramatsu@mizuho-rt.co.jp

DEPARTMENT OF MATHEMATICAL AND COMPUTING SCIENCE, SCHOOL OF COMPUTING, INSTITUTE OF SCIENCE TOKYO, 2-12-1, OOKAYAMA, MEGURO-KU, TOKYO 152-8552, JAPAN
Email address: sakie@c.titech.ac.jp

DEPARTMENT OF MATHEMATICAL AND COMPUTING SCIENCE, SCHOOL OF COMPUTING, INSTITUTE OF SCIENCE TOKYO, 2-12-1, OOKAYAMA, MEGURO-KU, TOKYO 152-8552, JAPAN